eNeuro

Research Article: New Research* | *Development

Integrative analysis of disease signatures shows inflammation disrupts juvenile experience-dependent cortical plasticity

Inflammation disrupts cortical plasticity

Milo R Smith[1–8], Poromendro Burman[1,3–5,8], Masato Sadahiro[1,3–6,8], Brian A Kidd[2,7], Joel T Dudley[2,7] and Hirofumi Morishita[1,3–5,8]

[1]*Department of Neuroscience*
[2]*Department of Genetics and Genomic Sciences*
[3]*Department of Psychiatry*
[4]*Department of Ophthalmology*
[5]*Mindich Child Health and Development Institute*
[6]*Graduate School of Biomedical Sciences*
[7]*Icahn Institute for Genomics and Multiscale biology*
[8]*Friedman Brain Institute*

DOI: 10.1523/ENEURO.0240-16.2016

Received: 9 August 2016

Revised: 1 November 2016

Accepted: 12 November 2016

Published: 15 December 2016

AUTHOR CONTRIBUTIONS M.R.S., B.A.K., H.M., and J.T.D. designed the study. M.R.S., P.B., M.S., and H.M. performed experiments. M.R.S., B.A.K., H.M. performed analyses. M.R.S., B.A.K., H.M., and J.T.D. wrote the paper.

Funding: NEI: EY024918; EY026053. Knights Templar Eye Foundation (KTEF): 100001209. march of dimes; HHS | NIH | National Institute of Child Health and Human Development (NICHD): 100000071; HD075735. NIEHS: ES023515. mindich child heath and development institute; Whitehall Foundation (Whitehall Foundation, Inc.): 100001391. NIH: DK098242; CA189201.

Correspondence should be addressed toCORRESPONDING AUTHOR Joel Dudley (joel.dudley@mssm.edu), Hirofumi Morishita (hirofumi.morishita@mssm.edu)

Cite as: eNeuro 2016; 10.1523/ENEURO.0240-16.2016

TITLE

Integrative analysis of disease signatures shows inflammation disrupts juvenile experience-dependent cortical plasticity

ABBREVIATED TITLE

Inflammation disrupts cortical plasticity

LIST OF AUTHORS

Milo R Smith[1-8] Poromendro Burman[1,3-5,8], Masato Sadahiro[1,3-6,8], Brian A Kidd[2,7], Joel T Dudley[2,7*], Hirofumi Morishita[1,3-5,8*]

AFFILIATIONS

Department of Neuroscience[1]

Department of Genetics and Genomic Sciences[2]

Department of Psychiatry[3]

Department of Ophthalmology[4]

Mindich Child Health and Development Institute[5]

Graduate School of Biomedical Sciences[6]

Icahn Institute for Genomics and Multiscale biology[7]

Friedman Brain Institute[8]

Icahn School of Medicine at Mount Sinai, 1 Gustave L Levy Place, New York NY, 10029

AUTHOR CONTRIBUTIONS

M.R.S., B.A.K., H.M., and J.T.D. designed the study. M.R.S., P.B., M.S., and H.M. performed experiments. M.R.S., B.A.K., H.M. performed analyses. M.R.S., B.A.K., H.M., and J.T.D. wrote the paper.

CORRESPONDING AUTHOR(S) EMAIL ADDRESS(ES)

Joel Dudley (joel.dudley@mssm.edu), Hirofumi Morishita (hirofumi.morishita@mssm.edu)

NUMBER OF FIGURES

4

NUMBER OF TABLES

3

NUMBER OF MULTIMEDIA

0

NUMBER OF WORDS, ABSTRACT

163

NUMBER OF WORDS, SIG STATEMENT

91

NUMBER OF WORDS, INTRO

430

NUMBER OF WORDS, DISCUSSION

1888

ACKNOWLEDGEMENTS

We thank Dr. N. Bukhari MD PhD for assistance with the gene expression experiments, Dr. B. Readhead MD for helpful discussions, and Dr. Nathaniel Heintz PhD (Rockefeller University) for providing Lynx1-/- mice.

CONFLICT OF INTEREST

Authors declare no competing financial interests

FUNDING SOURCES

Funded by Traineeship, NICHD-Interdisciplinary Training in Systems and Developmental Biology and Birth Defects T32HD075735 (M.R.S), Mindich Child Health and Development Institute Pilot Fund (J.T.D. and H.M.), P30 NIEHS Grant P30ES023515 (J.T.D and H.M.), R01EY024918 (H.M.), R01EY026053 (H.M.), Knights Templar Eye Foundation (H.M.), March of Dimes (H.M.), Whitehall Foundation (H.M.), R01DK098242 (J.T.D), and U54CA189201 (J.T.D).

ABSTRACT

Throughout childhood and adolescence, periods of heightened neuroplasticity are critical for the development of healthy brain function and behavior. Given the high prevalence of neurodevelopmental disorders such as autism, identifying disruptors of developmental plasticity represents an essential step for developing strategies for prevention and intervention. Applying a novel computational approach that systematically assessed connections between 436 transcriptional signatures of disease and multiple signatures of neuroplasticity, we identified inflammation as a common pathological process central to a diverse set of diseases predicted to dysregulate plasticity signatures. We tested the hypothesis that inflammation disrupts developmental cortical plasticity *in vivo* using the mouse ocular dominance model of experience-dependent plasticity in primary visual cortex. We found administration of systemic lipopolysaccharide suppressed plasticity during juvenile critical period with accompanying transcriptional changes in a particular set of molecular regulators within primary visual cortex. These findings suggest inflammation may have unrecognized adverse consequences on the postnatal developmental trajectory and indicates that treating inflammation may reduce the burden of neurodevelopmental disorders.

SIGNIFICANCE STATEMENT

During childhood and adolescence, heightened neuroplasticity allows the brain to reorganize and adapt to its environment. Disruptions in these malleable phases can result in permanent neurodevelopmental disorders. To identify pathological mechanisms that disrupt developmental neuroplasticity, we applied a systematic computational screen of hundreds of diseases for their impact on neuroplasticity. We discovered that inflammation would putatively disrupt neuroplasticity and validated this hypothesis in an *in vivo* experimental mouse model of developmental cortical plasticity. This work suggests that inflammation during the childhood period could have unrecognized negative consequences on the neurodevelopmental trajectory.

INTRODUCTION

During childhood and adolescence, the human brain undergoes tremendous reorganization during windows of heightened neuroplasticity. These windows of plasticity are *critical periods* that allow brain circuits to be refined by sensory and social experiences, which help establish normal perception and higher cognitive function (Johnson and Newport, 1989; Nikolopoulos et al., 1999; Lewis and Maurer, 2005; Schorr et al., 2005; Nelson et al., 2007; Fox et al., 2010). Disruption of these critical periods can alter neural circuits that shape function and behavior, which may, in turn, contribute to a wide range of psychiatric and neurodevelopmental disorders, such as autism (Weinberger DR, 1987; LeBlanc and Fagiolini, 2011; Takesian and Hensch, 2013; Lee et al., 2014). Previous studies focused on several genes relevant to autism spectrum disorders (*MeCP2, Ube3a, Fmr1*) and identified marked disruptions in developmental cortical plasticity (Tropea et al., 2009; Yashiro et al., 2009; Harlow et al., 2010). To our knowledge, no studies have conducted a systematic evaluation of pathological mechanisms that may disrupt developmental plasticity. The goal of this study was to leverage the growing repository of publically available transcriptome data from diverse disease states to identify pathological processes with the capacity to disrupt developmental cortical plasticity.

To identify pathological processes that disrupt developmental plasticity, we designed an integrative bioinformatics approach that identifies disruptive pathways through systematic evaluation of molecular profiles of disease states in humans and animals. Our approach adapts molecular matching algorithms from computational drug repurposing (for a review, see Hodos et al., 2016) to match transcriptional signatures of disease to those of neuroplasticity. To model plasticity, we leveraged the paradigmatic ocular dominance model of *in vivo* developmental plasticity (Wiesel and Hubel, 1963) and generated transcriptional signatures from primary visual cortex (V1). We matched plasticity and disease signatures to produce a diverse list of diseases ranked by their likelihood to dysregulate developmental plasticity. Across this ranked list, we sought to identify shared pathophysiology, rather than generate hypotheses about individual disease matches. To quantify shared pathophysiology, we developed and applied a novel Disease Leverage Analysis (DLA) that identifies shared molecular patterns of disease signatures to reveal novel disruptors of developmental plasticity. By examining shared pathophysiology, DLA identified a strong relationship between the molecular signatures of inflammation and developmental plasticity. We tested the hypothesis that inflammation disrupts developmental plasticity in the ocular dominance model of developmental V1 plasticity and found that functional, experience-dependent plasticity *in vivo* was suppressed by systemic inflammation. Our study demonstrates the utility of an integrative bioinformatics approach for identifying disruptors of developmental neuroplasticity and suggests that inflammation may be an unrecognized risk factor for neurodevelopmental disorders.

MATERIALS AND METHODS

Animals.

Male C57Bl6 mice (Charles River), and Lynx1$^{-/-}$ mice (Miwa et al., 2006) (gifted from Dr. Nathaniel Heintz, Rockefeller University), were group housed (3-5 animals per cage) under a standard 12 hr light:dark cycle (lights on at 7:00 AM:lights off at 7:00 PM) with constant temperature (23°C) and *ad libitum* access to food and water. The Institutional Animal Care and Use Committee at the Icahn School of Medicine at Mount Sinai approved all procedures involving animals.

Substances.

Lyophilized *Escherichia coli* lipopolysaccharide (LPS; serotype 0127:B8, Sigma-Aldrich Cat# L5024; Lot 073M4024V; 600,000 EU/mg) was reconstituted in sterile saline (0.9% NaCl) to yield a stock solution of 2 mg/mL, which was diluted with saline on the day of injection to yield a working concentration of 0.03 mg/mL.

Plasticity signature generation.

Transcriptomes were profiled with microarray to generate plasticity signatures. Experiment-naive juvenile C57Bl6 at postnatal day 29 (P29), adult Lynx1$^{-/-}$ (> P60), and adult C57Bl6 (> P60) mice (n = 3 each group) were anesthetized with isoflurane, cervically dislocated, bilateral primary visual cortex (V1) was removed, immediately frozen on dry ice, and stored at -80° C until processed. Total RNA was extracted from V1 using RNeasy Lipid Tissue Mini kit (Qiagen) and stored at -80° C. 4.5 μg of RNA was hybridized to

Illumina WG-6 2.0 microarrays (750 ng per subarray). A juvenile plasticity signature was generated via differential expression analyses of juvenile versus adult V1 transcriptomes by first quantile normalizing probe-level data with Limma (Smyth, 2005) and then computing rank-based differential expression with RankProd (Hong et al., 2006) (both R packages available through the Bioconductor repository) to yield 193 unique mouse Entrez IDs. For downstream analysis, mouse Entrez IDs were mapped to human orthologues using the Mouse Genome Informatics homology reference to yield a 176 gene juvenile plasticity signature. We generated a Lynx1$^{-/-}$ signature in an analogous manner to juvenile, to yield a Lynx1$^{-/-}$ plasticity signature of 98 genes.

Molecular matching algorithm.

To identify diseases that are predicted to dysreguate plasticity signature genes, we developed a molecular matching score, which is the sum of the absolute value of the rank-difference gene expression measure of disease signatures (see Dudley et al., 2009 for details of this expression measure) that intersect with neuroplasticity signature genes. The absolute value was chosen to simplify downstream interpretation. This score is similar in spirit to the approach taken by Zhang and Gant (2008), except in our implementation high scores indicate significant overlap between disease and plasticity signatures whereas low scores indicate little or no overlap. To compare match scores (M) across diseases, we normalized the scores with n = 10,000 permutations of scores using $\frac{M_{actual} - \bar{M}_{perm}}{\sqrt{\frac{\sum_{i=1}^{n}(M_{perm_i} - \bar{M}_{perm})^2}{n-1}}}$. P-values were estimated using the Generalized Pareto Distribution (Knijnenburg et al., 2009) on n permutations and were multiple-test corrected using the Benjamini and Hochberg method (Benjamini and Hochberg, 1995).

Disease Leverage Analysis (DLA).

We developed DLA to infer pathological processes that are shared across diseases and predicted to dysregulate plasticity signature genes. For pathological processes, we used the 50 “hallmark” gene sets (MSigDb) (Subramanian et al., 2005). We computed a pathology score for each hallmark gene set for each disease signature, for a total of 50 × 436 = 21,800 scores. A pathology score is the sum of the absolute value of the normalized disease signature gene expression that is shared with a hallmark gene set. The absolute value was chosen because the direction of effect for gene sets is not necessarily known. We next calculated a linear regression between the pathology scores for a specific gene set and the plasticity-disease molecular match scores. We estimated the p-value for the association between the pathology scores and disease-plasticity scores (the β_1 coefficient) by computing 20,000 permutations of pathology scores using gene sets the same length as the input gene set and then calculating the regression on the permuted scores. If $\sum_{i=1}^{n}[\mathbb{1}_{[\,|\beta1_{perm_i}|>|\beta1_{actual}|\,]}] > 10$, where $\mathbb{1}$ is the indicator function (i.e. the value is 1 when the conditional is satisfied and 0 otherwise) and n = the number of permutations, the p-value was the empirical estimate: $\frac{\sum_{i=1}^{n} |\beta1_{perm_k}|>|\beta1_{actual}|}{n}$; otherwise, the Generalized Pareto Distribution was used to estimate the p-value (Knijnenburg et al., 2009). The Bonferroni method was used to correct for multiple hypothesis tests (denoted $p_{corrected}$ in the text). To account for the probability of a large coefficient by chance, actual β_1

coefficients were normalized by the permutated distribution of β_1 according to $\frac{\beta1_{actual} - \overline{\beta1}_{perm}}{\sqrt{\frac{\sum_{i=1}^{n}(\beta1perm_i - \overline{\beta1}perm)^2}{n-1}}}$. Positive βs are pathological processes associated with diseases that predicted to disrupt plasticity signatures. Negative β s are pathological processes associated with diseases that are predicted to *not* disrupt plasticity signatures. To calculate enrichments of top DLA gene sets, we chose a conservative cutoff of $p_{corrected} < 5 \times 10^{-5}$ and then calculated the overrepresentation of inflammation gene sets among positive DLA associations. To do so, we used the hypergea (Bönn, 2016) R package, which uses a conditional maximum likelihood estimate to compute the odds ratio on adjusted cell counts (to avoid empty cells) and obtains two-sided p-values from the hypergeometric distribution.

Quantitative PCR.

Experiment-naive juvenile mice (P26, n = 5 per group) were lightly anesthetized with isoflurane to avoid additional stressors and injected intraperitoneal (i.p.) before 12:00 noon EST with a dose of LPS that does not cross the blood-brain barrier (Banks and Robinson, 2010) (300 µg/Kg, ~4.5 µg/mouse) or vehicle (150 µL saline). 4h later mice were deeply anesthetized with isoflurane, decapitated, and bilateral V1 was removed under RNAse free conditions, briefly rinsed in sterile saline (0.9% NaCl), immediately frozen on dry ice, and transferred to -80°C until processed. Total RNA was extracted from V1 using RNeasy Lipid Tissue Mini kit (Qiagen) and stored at -80°C. RNA yields ranged from 4.5-10 μ g per sample and RINs ranged from 8.7-10 (mean 9.8, sd 0.32). Total V1 RNA was converted to cDNA using High-Capacity cDNA Reverse Transcription Kit (Life

Technologies). qPCR was carried out by the Mount Sinai Quantitative PCR core facility using TaqMan probes (Applied Biosystems; Catalog Numbers: *NogoR*: 00445861, *Lynx1*: 01204957_g1, *S100a8*: 00496696_g1, *Lrg1*: 01278767_m1, *Lcn2*: 01324470_m1, *PirB*: 01700366_m1, *Cldn5*: 00727012_s1, *Egr2*: 00456650_m1, *Npas4*: 01227866_g1, Il1: 00434228_m1, *Agmat*: 01348862_m1, *Ch25h*: 00515486_s1, *Alox12b*: 01325300_gH, *Evpl*: 01700609_m1, *Slc40a1*: 00489835_g1, *Arc*: 01204954_g1, *S100a9*: 00656925_m1, *H2D1/H2K1*: 04208017_mH, *BDNF*: 04230607_s1, *Nptx2*: 00479438_m1, *Ppp3ca*: 01317678_m1). Quantification of fold change was derived via the $-\Delta\Delta$CT method (equivalent to a log2 fold change) and significance was computed with parametric *t*-tests of the ΔCTs, given the approximately normal distribution of ΔCTs. To prioritize qPCR validations, we identified the most differentially dysregulated juvenile neuroplasticity genes by an independent LPS-brain study (GSE3253) by subsetting with the LPS-brain expression whose absolute expression statistic was greater or equal to 2 after conversion to Z-score.

***In vivo* electrophysiology.**

Under light isoflurane anesthesia, the contralateral eye of experiment-naive P26 mice was sutured and the animal was immediately injected i.p. with LPS (300 μg/Kg, ~4.5 μg/mouse) or vehicle (150 μL saline). 3d later, single unit electrophysiological recordings were taken in binocular zone of V1 in response to visual stimuli presented to each eye separately(Gordon and Stryker, 1996). Briefly, recording was conducted under nembutal/chlorprothixene anesthesia. Visually evoked single-unit responses were recorded with 16-channel silicone probes (Neuronexus) in response to a high contrast single bar generated by visage system (Cambridge Research Systems). The signal was amplified and thresholded (OmniPlex, Plexon). To ensure single-unit isolation, the waveforms of recorded units were further examined offline (Offline Sorter, Plexon). For each animal, approximately 3 to 10 single units were recorded in each of the 4 to 6 vertical penetrations spaced evenly (250 µm intervals) across the mediolateral extent of V1 to map the monocular and binocular zones and avoid sampling bias. Monocular zone was identified when three consecutive units registered solely contra-responses within a single penetration (ODS of 1, see below for definition of ODS). Secondary visual cortex was identified by the reversal of retinotopy seen as the electrode was moved into the secondary visual cortex (Gordon and Stryker, 1996). Mice that experienced opening of the sutured eye or that had poor recordings (< 10 cells/mouse or < 3 penetrations / mouse or lack of positive identification of monocular zone and secondary visual cortex) were excluded from further study. To analyze the electrophysiology data, normalized ocular dominance index (ODI) of single neurons was computed by a custom made MATLAB code by peristimulus time histogram analysis of peak to baseline spiking activity in response to each eye: {[Peak(ipsi)-baseline (ipsi)]–[Peak (contra)-baseline(contra)]}/{[Peak (ipsi) – base line(ipsi)]+ [Peak(contra)-baseline(contra)]}, which produces a range of [-1,+1] where -1 is a completely contra-dominated cell and +1 is a completely ipsi-dominated cell. ODI is linearly transformed by assigning [-1.0, -0.5) = **1,** [-0.5, -0.3) = **2**, [-0.3, -0.1) = **3**, [-0.1, +0.1] = **4**, (+0.1, +0.3] = **5**, (+0.3, +0.5] = **6**, (+0.5, +1.0] = **7** to produce the ocular dominance score (ODS). Finally, the contralateral bias index (CBI), a monocular weighted, animal-level summary statistic, is computed from the ODS: [(n**1**-n**7**)+2/3(n**2**-n**6**)+1/3(n**3**-n**5**)+N]/2N, where N=total number of cells and n**x**=number of cells corresponding to ocular dominance score of **x**. Thus, CBI of 0.7 is contra-dominant and a CBI of 0.4 is ipsi-dominant. For statistical comparison of ocular dominance, ODS of single neurons were plotted as a proportion histogram and compared via the non-parametric Chi-squared test and CBI of single animals were compared via *t*-test. Saline-treated juvenile animals (P26) were the comparison group. The experimenter was blind to the sample group. Sample sizes were statistically estimated prior to undertaking experimental work to be n = 6 per group, assuming effect sizes seen in previous relevant work.

Statistical Analysis

All statistical and computational analyses conducted with R (Version 3.2.2) and Python (Version 2.7.10). Parametric Welch *t*-tests were two-sided, unless otherwise noted. Sample sizes (denoted n) always indicate the number of mice. Influenza 95% confidence interval for the incidence rate ratio (IRR) was estimated using the Katz log approach (Fagerland et al., 2015) ($e^{log(IRR) \pm \sqrt{\frac{1}{a}+\frac{1}{b}-\frac{1}{m}-\frac{1}{n}}}$) where *a* and *b* are the successes and *m* and *n* are the totals (totals determined by dividing the successes by the published incidence rates).

Statistical Table

Subscript	Data structure	Type of test	Power
a	hypergeometric	Fisher's Exact	95%CI = [1.4, 491.2]
b	hypergeometric	Fisher's Exact	95%CI = [23.8, 58.0]
c	hypergeometric	Fisher's Exact	95%CI = [3.2, 1,229.8]
d	approx. normal	Welch *t*-test	95%CI = [-3.3, -1.6], alternative hypothesis: true difference in means is not equal to 0.
e	non-normal	empirical p-value	NA

f	non-normal	Spearman rank correlation	NA
g	approx. normal.	Welch *t*-test	NA - no specific p-values reported, rather a group of genes under specified p-value threshold.
h	approx. normal.	Welch *t*-test	95%CI = [-3.0, -0.1] , alternative hypothesis: true difference in means is not equal to 0.
i	approx. normal.	Welch *t*-test	95%CI = [-1.3, -0.1] , alternative hypothesis: true difference in means is not equal to 0.
j	approx. normal.	Welch *t*-test	95%CI = [0.3, 1.6], alternative hypothesis: true difference in means is not equal to 0.
k	approx. normal	Welch *t*-test	NA - no specific p-values reported, rather a group of genes above specified p-value threshold (e.g. not significant).
l	approx. normal.	Welch *t*-test, one-sided (due to specific prior hypothesis as to direction of effect; results still significant using a two-sided test at a threshold of α=0.05)	95%CI = [0.1, Inf], alternative hypothesis: true difference in means is not equal to 0.
m	non-normal	χ^2 test of ODS counts	NA

RESULTS

Molecular matching between plasticity and disease signatures

To enable molecular matching between plasticity and disease, we compared V1 transcriptomes of juvenile wild-type mice, during the critical period of elevated ocular dominance plasticity in V1 (Gordon and Stryker, 1996), to adult wild-type mice with reduced plasticity, to identify a differential expression signature of 176 genes **(Figure 1a and Table 1).** We computationally matched this signature to 436 disease signatures derived from public microarray data using a previously described method (Dudley et al., 2009) **(Figure 1a).** This systematic method applies a rank-based molecular matching algorithm to determine the molecular concordance between the plasticity signature and a given disease signature, where high scores indicate plasticity genes are significantly dysregulated by the disease and low scores indicate that the disease has no impact on plasticity genes (for details, see Materials and Methods) **(Figure 1b).** The molecular matching procedure produced a list of 436 diseases ordered by their prediction to disrupt the plasticity signature **(Table 2).** Interestingly, highly ranked diseases included not only brain disorders known to disrupt plasticity such as Huntington's Disease (Usdin et al., 1999; Murphy et al., 2000; Milnerwood et al., 2006), but also non-neurologic disorders (e.g. bacterial infections, inflammatory bowel disease, metabolic diseases), suggesting a broad range of disease states may impact molecular pathways involved in plasticity.

Disease Leverage Analysis identifies inflammatory processes as putative disruptors of plasticity

We sought to identify shared pathophysiology across the diverse list of diseases predicted to dysregulate plasticity signatures. To do so, we developed an approach called Disease Leverage Analysis (DLA). This approach calculates the association between diseases that dysregulate the plasticity signature genes and the 50 gene sets in the "hallmark" library (Subramanian et al., 2005) that represent well-defined and distinct biological pathways. Specifically, DLA computes a linear regression between the molecular match score (a measure of strength of association between disease and plasticity signatures) and the pathology score (a measure of activity of the biological pathway in a given disease). Large regression coefficients indicate that a given biological pathway is highly active in diseases that dysregulate plasticity gene signatures and may be pathological to developmental plasticity. Using a multiple-test corrected, empirical p-value threshold of $p < 5 \times 10^{-5}$, we found that 7 of 14 largest DLA associations were inflammation-related gene sets and that every inflammation-related gene set in the hallmark library was strongly associated with diseases that dysregulate the plasticity signature (7/7 inflammation gene sets at a threshold of $p_{corrected} < 5 \times 10^{-5}$: OR = 25.8, 95% CI = [1.4, 491.2], $p = 2.7 \times 10^{-3}$[a], Fisher's Exact Test) **(Figure 1c and Figure 1-1)**. Moreover, 2 of these gene sets, TNF-α signaling via NFκB and IFN-γ response, reflect pathways involved in critical period plasticity (Kaneko et al., 2008; Nagakura et al., 2014).

To control for non-plasticity aspects of age, we repeated the entire analysis using a Lynx1$^{-/-}$ plasticity signature of 98 genes, identified by computing the differential expression between adult Lynx1$^{-/-}$ and adult wild-type V1 **(Table 3)**. By releasing the Lynx1 brake on plasticity, Lynx1$^{-/-}$ mice have juvenile-like plasticity in adulthood (Morishita et al., 2010;

Bukhari et al., 2015). Indeed, functional similarity is reflected in signature similarity, as juvenile and Lynx1-KO plasticity signatures significantly overlap (35 genes shared, OR = 37.1, 95% CI = [23.8, 58.0], $p < 2.2 \times 10^{-16}{}_{b}$). Using DLA on the Lynx1$^{-/-}$ molecular matches, we found a strong association between diseases predicted to disrupt Lynx1$^{-/-}$ plasticity and inflammation-related gene sets (7/7 inflammation gene sets at a threshold of $p_{corrected} < 5 \times 10^{-5}$: OR = 63.0, 95% CI = [3.2, 1,229.8], $p = 7.6 \times 10^{-5}{}_{c}$ Fisher's Exact Test) **(Figure 2 and Figure 2-1)**. Together, the bioinformatics analyses indicate that inflammation is a process central to diseases predicted to dysregulate plasticity gene expression, suggesting that inflammation may disrupt developmental plasticity.

Lipopolysaccharide model of inflammation suppresses developmental cortical plasticity

Based on the DLA findings, we hypothesized that inflammatory processes disrupt developmental cortical plasticity. To test this hypothesis, we induced a systemic inflammatory response via lipopolysaccharide (LPS) and measured the impact on developmental plasticity and related gene expression. We injected a low dose of LPS (300 μg/Kg) intraperitoneal (i.p.) at the peak of juvenile ocular dominance plasticity at postnatal day 26 (P26) and found a strong inflammatory response in V1, as indicated by a 2.4 $\log_2$ fold-increase of *Il-1β* compared to vehicle control ($p = 3.4 \times 10^{-4}{}_{d}$, *t*-test of ΔCTs, n = 5 mice per group). To identify a focused subset of plasticity genes likely to be regulated by LPS (regardless of age or specific brain region) to test *in vivo*, we investigated a highly significant molecular match between the juvenile plasticity signature and an adult brain-derived LPS transcriptome (GSE3253; rank #14, $p = 7.9 \times 10^{-4}{}_{e}$; empirical p-value calculated using molecular match algorithm) **(Table 2 and Figure 3a).** Next, we identified a subset of genes from GSE3253 likely to play a larger role in the underlying biology (the genes in the extremes using a Z-score cutoff) and intersected it with the plasticity signature to identify 16 shared genes **(Figure 3b).** Notably, among these shared genes we identified a negative correlation in their expression pattern (cor = -0.77, $p = 0.0007_{f}$, Spearman correlation). Among these 16 shared genes, the adult LPS data indicated the direction of expression of 13 would be reversed by LPS. Indeed, the majority (61.5%) of the 13 genes showed a complete reversal in their differential expression pattern in V1 after peripheral LPS administration during the critical period (qPCR, all reversed genes $p < 5 \times 10^{-4}{}_{g}$, *t*-test of ΔCTs, n = 5 mice per group) **(Figure 3c).** This data indicates that genes in the plasticity signature that are also regulated by LPS act in an antagonistic fashion, and naturally led us to the hypothesis that inflammation may *suppress* plasticity. Consistent with this logic, the established brakes of plasticity, Pirb (Syken et al., 2006) and H2K1 & H2D1 (Datwani et al., 2009), showed increased expression compared to vehicle ($p = 0.04_{h}$, $p = 0.03_{i}$ respectively, *t*-test of ΔCTs, n = 5 mice per group) **(Figure 4a-b).** In addition, a trigger of plasticity that increases across development, BDNF (Huang et al., 1999), which we predicted *in silico* to decrease after LPS **(Figure 3b)**, showed decreased expression compared to vehicle ($p = 0.009_{j}$, *t*-test of ΔCTs, n = 5 mice per group) **(Figure 4b).** In contrast, other known plasticity effectors (Takesian and Hensch, 2013) were not changed relative to vehicle (Nptx2, Lynx1, NogoR, Ppp3ca; $p > 0.1_{k}$, *t*-test of ΔCTs, n = 5 mice per group) indicating that LPS may act through a specific subset of known and novel plasticity effectors **(Figure 4b)**.

Finally, we tested if inflammation suppresses experience-dependent developmental cortical plasticity *in vivo*. We administered LPS (300 μg/Kg i.p.) or saline on P26 immediately after suturing one eye to induce ocular dominance plasticity via monocular deprivation (MD) **(Figure 4a).** After three days of MD, we conducted *in vivo* single unit recordings of activity-driven changes in eye preference of single neurons (ocular dominance) in binocular V1 in response to light (Gordon and Stryker, 1996). In mice treated with saline, we observed the expected shift in cortical responsivity to light stimulation from the deprived contralateral to non-deprived ipsilateral eye, as quantified by a decrease in the animal-level contralateral bias index (CBI) (CBI=0.49 ± 0.04, 6 mice, 135 cells), indicating the presence of developmental plasticity **(Figure 4c, right hand plot).** In contrast, LPS significantly suppressed the shift in cortical responsivity from the deprived contralateral eye to the non-deprived ipsilateral eye, quantified by an increase in CBI and an elimination of the right shift in distribution of ocular dominance scores (ODS) of single neurons (CBI = 0.64 ± 0.02, 7 mice, 129 cells; one-sided *t* test of CBIs: $p = 0.006_{l}$; χ^2 test of ODS distribution: $p = 2.6 \times 10^{-6}{}_{m}$), indicating impaired plasticity during the critical period in V1 **(Figure 4c, left hand plot).** Taken together, these data are consistent with our informatics-derived hypothesis by demonstrating that peripheral injection of LPS induces an inflammatory response in the brain and suppresses developmental cortical plasticity *in vivo.*

DISCUSSION

Using an integrative bioinformatics approach, we found that inflammation disrupts developmental cortical plasticity. Our study demonstrates the utility of this approach for both identifying diseases that may disrupt plasticity and generating hypotheses on the molecular mechanisms underlying these disruptions. Moreover, our novel Disease Leverage Analysis facilitates novel hypothesis generation, because seemingly unrelated phenotypes, such as neuroplasticity and inflammation, can be connected based on apparently disparate tissues and diseases. Previous work indicating that the disease signal harmonizes across tissues (Dudley et al., 2009) support this approach, and in the present study suggests that the molecular pathways underlying plasticity are shared in diverse tissues and dysregulated in many disease states, including apparently non-neurological phenotypes (e.g. bacterial infections, inflammatory bowel disease, metabolic diseases). Importantly, the biological relevance of any given molecular match between plasticity and disease must be interpreted with care. In all cases, molecular matches indicate that plasticity and the disease phenotype share underlying molecular machinery. However, a given disease state in a specific tissue may or may not have an impact on functional plasticity or related gene expression if the disease state or tissue is sufficiently localized and segregated from neural tissue. Consequently, we developed Disease Leverage Analysis to use the information of all matches collectively to identify common disease processes and simultaneously shrink the hypothesis space to a manageable set of disease process-oriented hypotheses that bind together the diverse matches. This approach facilitated the unbiased and systematic use of apparently disparate disease signatures to generate novel hypotheses about shared disease mechanisms that may dysregulate plasticity. We find here that a common theme among these dysregulations is inflammation, a biological process well-suited to communicate peripheral signals to the brain, disrupting plasticity.

We demonstrate several lines of evidence supporting a hypothesis that plasticity and inflammatory processes share components of underlying molecular networks. We computationally predicted associations between plasticity signature-perturbing diseases and TNF-α and IFN-γ pathways (Figure 1 and 2) and also experimentally identified associations between systemic inflammation and increases in the plasticity brakes Pirb and MHC-I in the brain (Figure 4). These predictions and observations confirm the known role of pathways involving TNF-α, IFN-γ, Pirb, and MHC-I on regulating developmental plasticity (Syken et al., 2006; Kaneko et al., 2008; Datwani et al., 2009; Nagakura et al., 2014) and extend them to the context of inflammation. We also showed that BDNF, a neurotrophic factor essential to the opening of the critical period (Huang et al., 1999), is decreased after LPS (Figure 4), which is consistent with the reported antagonistic relationship of peripheral LPS on brain BDNF (Guan and Fang, 2006; Schnydrig et al., 2007). Interestingly, we also found that the microglial activator Lcn2 (Jang et al., 2013) is a member of both the juvenile and Lynx1$^{-/-}$ plasticity signatures (Tables 1 and 3) and is dramatically increased after LPS in V1 during the critical period (Figure 3). Activation may inhibit microglia from carrying out their "resting-state" role in mediating experience-dependent plasticity (Sipe et al., 2016), contributing to the dampening of plasticity by inflammation. Collectively, our work suggests a conflict between developmental cortical plasticity and immune-related molecular networks during inflammation, ultimately resulting in suppression of plasticity during inflammation. Our study provides a novel subset of transcripts that can be used to guide future mechanistic studies into inflammation-plasticity interactions.

Our efforts to understand the molecular machinery involved in suppression of developmental plasticity focused on immediate changes in gene expression in V1 via acute inflammation (qPCR 4h after a single i.p. injection of LPS). We expected this time point to be particularly sensitive to disruption because the earliest experience-dependent changes occur within hours to a day of MD at the level of firing rate of parvalbumin interneurons (Aton et al., 2013; Kuhlman et al., 2013; Reh and Hensch, 2014) and protease (Mataga et al., 2002) and microglia activity (Sipe et al., 2016) as triggers for subsequent global ocular dominance plasticity, which takes a few days to be detected by single unit recordings (Gordon and Stryker 1996). Importantly, such trigger events only occur during juvenile critical period when our assay was performed, but not in the adult (Kuhlman et al., 2013). Thus, we reasoned that the baseline cortical expression signature at this early time point would be critical to gate global ocular dominance plasticity. In addition, peak acute inflammatory response as measured by increase in Il1β in brain after peripheral LPS injection is between 1-4h (Layé et al., 1994; Eklind et al., 2006; Richwine et al., 2009), a time-course well-suited to disrupt these earliest experience-dependent plasticity events. While we speculate that LPS disrupted these early trigger events unique to juvenile cortex, more work needs to be carried out to understand the molecular events underlying the functional changes seen within hours of MD and to dissect the impact of inflammation on these events. In addition to the early phase of plasticity, inflammation may also impact plasticity mechanisms during the later phases of MD because TNF-α is essential to non-deprived eye potentiation via a homeostatic mechanism at 5-6d of MD (Kaneko et al., 2008). Ultimately, further work is necessary to tease out the interaction between inflammatory and plasticity mechanisms that contribute to suppression of functional plasticity across multiple days of experience deprivation. Performing such work comparing acute versus chronic inflammatory models would provide fascinating insights into neuroimmune biology and would help inform the important clinical question of the potential impact of acute and chronic inflammation on the neurodevelopmental trajectory in children.

While our experimental efforts focused on the impact of acute inflammation on plasticity, our list of diseases predicted to impact plasticity include diseases that accompany chronic inflammation (Table 2). Efforts studying human disease and animal models may shed light on how acute versus chronic inflammation effects plasticity. For example, components of plasticity and inflammation are dysregulated in epilepsy (Vezzani and Granata, 2005). Acute inflammation from low to high doses (LPS) decreases the threshold for induction of seizure (Sayyah et al., 2003) and a single early life inflammatory insult increases susceptibility to seizure even into adulthood (Galic et al., 2008). Chronic overexpression of inflammation-related genes in rodents causes an increased or decreased susceptibility to seizure, depending on gene dose (Vezzani and Granata, 2005) and seizure itself appears to chronically induce inflammatory markers (De Simoni et al., 2000). This evidence indicates a potential bidirectional effect of epilepsy and inflammation, wherein acute and chronic inflammation may have immediate and long term effects on epilepsy-related plasticity mechanisms. In addition to epilepsy, cortical lesions and hypoxia-ischemia induce a robust inflammatory response that can endure chronically (Bona et al., 1999; Schroeter et al., 2002) and disrupt ocular dominance plasticity weeks after the injury (Failor et al., 2010; Greifzu et al., 2011). Interestingly, anti-inflammatory (ibuprofen) treatment rescues MD-induced sensory learning (increased visual acuity of the non-deprived eye) in adult (P70-110) after cortical injury via photothrombosis in the nearby primary somatosensory; however, ibuprofen did not restore ocular dominance plasticity (Greifzu et al., 2011). It is possible that the anti-inflammatory regimen or mechanism of action used was not sufficient to eliminate the inflammation and rescue ocular dominance plasticity, or it may reflect distinct mechanisms of plasticity and their modulation by inflammation in the juvenile cortex versus the adult. While it has been proposed that causes of plasticity disruption may be cortical deafferentiation in the case of cortical lesions or disruption of inhibitory interneurons in the case of hypoxia-ischemia, it is possibile that inflammation downstream of injury disrupts plasticity and should be investigated further. In sum, there is evidence that chronic and acute inflammation go hand in hand with disrupted plasticity across a variety of brain disorders, on different time scales, and as a function of different underlying mechanisms. Going forward, work is necessary to understand the contribution of diverse inflammatory mechanisms in the disruption of various types of plasticity across a wide variety of neurological and neurodevelopmental conditions.

Our finding that inflammation suppresses developmental cortical plasticity suggests a potential public health concern related to neurodevelopmental trajectory. During the height of the critical period for visual plasticity (peak is 0.5-2 years in humans (Morishita and Hensch, 2008)), children < 5 years have the highest incidence of contracting LPS-carrying gram-negative foodborne pathogens relative to other childhood or adult periods (Centers for Disease Control and Prevention (CDC), 2013). Other infections that induce inflammation also show an increased incidence during the peak of developmental plasticity in humans; > 80% of children < 3 years experience otitis media (ear infection) (Marom et al., 2014) and children < 5 years are hospitalized for influenza-related complications nearly an order of magnitude more often than children 5-17 years (Incidence Rate Ratio = 8.1, 95% CI = [7.3, 9.0]) [Data from (Dawood et al., 2010)]. Our work suggests this increased incidence of infection during postnatal periods of developmental plasticity (relative to older ages) may be an unrecognized mechanism by which inflammation alters the neurodevelopmental trajectory. Most directly, suppression of visual cortex plasticity could disrupt the development of binocular matching (Wang et al., 2010), a process central to the development of normal vision and which specifically depends on heightened plasticity during the critical period for visual development. In addition, higher-order cognitive processes could be disrupted, due to the hierarchical dependency of various critical periods of plasticity (Takesian and Hensch, 2013). In addition, given that mechanisms of plasticity identified in the visual critical period have translated to other brain regions and functions (Levelt and Hübener, 2012; Nabel and Morishita, 2013; Werker and Hensch, 2015), it is likely that inflammation could disrupt plasticity in other systems.

Our work is a natural extension to the *postnatal* epoch of the growing body of research indicating deleterious brain and behavioral outcomes due to *prenatal* inflammatory exposure (Steullet et al., 2014; Choi et al., 2016; Weber-Stadlbauer et al., 2016) and suggests that inflammation may have a more extensive impact on *postnatal* neurodevelopment and brain function than previously realized. In fact, childhood infections and inflammation are associated with subsequent diagnoses of autism, depression, and schizophrenia as well as declines in cognitive capacity (Atladóttir et al., 2010; Khandaker GM et al., 2014; Dalman et al., 2008; Benros et al., 2015). The elevated incidence rate of infections during childhood neurodevelopment (relative to older ages) and association of childhood infection with subsequent neurodevelopmental disorder may indicate a partial explanation for the observed onset of psychiatric disorder in childhood and adolescence (Lee et al., 2014). Our work showing that inflammation disrupts developmental cortical plasticity suggests an unrecognized risk factor for neuropsychiatric disorder and provides a starting point to investigate the underlying pathophysiology.

We show here that an integrative bioinformatics approach is well-suited to interrogate the interactions between disease processes and disruptions in developmental plasticity. To extend this approach further, molecular matching could be expanded to the > 71,000 experiments publically available (as of 2016 August 04, there were 71,885 Gene Expression Omnibus "Series") and Disease Leverage Analysis could be expanded to the universe of biologically-defined gene sets (as of 2016 August 04, MSigDb alone contained 13,311 sets), facilitating more comprehensive interrogation of the disease space and generation of more specific hypotheses about disease processes that disrupt plasticity. Moreover, this approach is not limited to interrogating neurodevelopment, but can be extended to other neurological signatures beyond plasticity. We expect it will be useful for identifying connections between disease processes and other brain phenotypes that can be appropriately represented by a transcriptional signature.

REFERENCES

Atladóttir, HO, Thorsen, P, Schendel, DE, Østergaard, L, Lemcke, S, Parner, ET. 2010. Association of hospitalization for infection in childhood with diagnosis of autism spectrum disorders: a Danish cohort study. Arch. Pediatr. Adolesc. Med. 164: 470–477.

Aton, SJ, Broussard, C, Dumoulin, M, Seibt, J, Watson, A, Coleman, T, Frank, MG. 2013. Visual experience and subsequent sleep induce sequential plastic changes in putative inhibitory and excitatory cortical neurons. Proc. Natl. Acad. Sci. 110: 3101–3106.

Banks, WA, Robinson, SM. 2010. Minimal penetration of lipopolysaccharide across the murine blood–brain barrier. Brain. Behav. Immun. 24: 102–109.

Benjamini, Y, Hochberg, Y. 1995. Controlling the False Discovery Rate: A Practical and Powerful Approach to Multiple Testing. J. R. Stat. Soc. Ser. B Methodol. 57: 289–300.

Benros, ME, Sørensen, HJ, Nielsen, PR, Nordentoft, M, Mortensen, PB, Petersen, L. 2015. The Association between Infections and General Cognitive Ability in Young Men – A Nationwide Study. PLOS ONE 10: e0124005.

Bona, E, Andersson, A-L, Blomgren, K, Gilland, E, Puka-Sundvall, M, Gustafson, K, Hagberg, H. 1999. Chemokine and Inflammatory Cell Response to Hypoxia-Ischemia in Immature Rats. Pediatr. Res. 45: 500–509.

Bönn, M. 2016. hypergea: Hypergeometric Tests. Version 1.2.3.

Bukhari, N, Burman, PN, Hussein, A, Demars, MP, Sadahiro, M, Brady, DM, Tsirka, SE, Russo, SJ, Morishita, H. 2015. Unmasking Proteolytic Activity for Adult Visual Cortex Plasticity by the Removal of Lynx1. J. Neurosci. 35: 12693–12702.

Centers for Disease Control and Prevention (CDC). 2013. Incidence and trends of infection with pathogens transmitted commonly through food - foodborne diseases active surveillance network, 10 U.S. sites, 1996-2012. MMWR Morb. Mortal. Wkly. Rep. 62: 283–287.

Choi, GB, Yim, YS, Wong, H, Kim, S, Kim, H, Kim, SV, Hoeffer, CA, Littman, DR, Huh, JR. 2016. The maternal interleukin-17a pathway in mice promotes autism-like phenotypes in offspring. Science 351: 933–939.

Dalman, C, Allebeck, P, Gunnell, D, Harrison, G, Kristensson, K, Lewis, G, Lofving, S, Rasmussen, F, Wicks, S, Karlsson, H. 2008. Infections in the CNS During Childhood and the Risk of Subsequent Psychotic Illness: A Cohort Study of More Than One Million Swedish Subjects. Am. J. Psychiatry 165: 59–65.

Datwani, A, McConnell, MJ, Kanold, PO, Micheva, KD, Busse, B, Shamloo, M, Smith, SJ, Shatz, CJ. 2009. Classical MHCI Molecules Regulate Retinogeniculate Refinement and Limit Ocular Dominance Plasticity. Neuron 64: 463–470.

Dawood, FS, Fiore, A, Kamimoto, L, Bramley, A, Reingold, A, Gershman, K, Meek, J, Hadler, J, Arnold, KE, Ryan, P, Lynfield, R, Morin, C, Mueller, M, Baumbach, J, Zansky, S, Bennett, NM, Thomas, A, Schaffner, W, Kirschke, D, Finelli, L. 2010. Burden of Seasonal Influenza Hospitalization in Children, United States, 2003 to 2008. J. Pediatr. 157: 808–814.

De Simoni, MG, Perego, C, Ravizza, T, Moneta, D, Conti, M, Marchesi, F, De Luigi, A, Garattini, S, Vezzani, A. 2000. Inflammatory cytokines and related genes are induced in the rat hippocampus by limbic status epilepticus. Eur. J. Neurosci. 12: 2623–2633.

Dudley, JT, Tibshirani, R, Deshpande, T, Butte, AJ. 2009. Disease signatures are robust across tissues and experiments. Mol. Syst. Biol. 5.

Eklind, S, Hagberg, H, Wang, X, Sävman, K, Leverin, A-L, Hedtjärn, M, Mallard, C. 2006. Effect of Lipopolysaccharide on Global Gene Expression in the Immature Rat Brain. Pediatr. Res. 60: 161–168.

Fagerland, MW, Lydersen, S, Laake, P. 2015. Recommended confidence intervals for two independent binomial proportions. Stat. Methods Med. Res. 24: 224–254.

Failor, S, Nguyen, V, Darcy, DP, Cang, J, Wendland, MF, Stryker, MP, McQuillen, PS. 2010. Neonatal Cerebral Hypoxia–Ischemia Impairs Plasticity in Rat Visual Cortex. J. Neurosci. 30: 81–92.

Fox, SE, Levitt, P, Nelson III, CA. 2010. How the Timing and Quality of Early Experiences Influence the Development of Brain Architecture. Child Dev. 81: 28–40.

Galic, MA, Riazi, K, Heida, JG, Mouihate, A, Fournier, NM, Spencer, SJ, Kalynchuk, LE, Teskey, GC, Pittman, QJ. 2008. Postnatal Inflammation Increases Seizure Susceptibility in Adult Rats. J. Neurosci. 28: 6904–6913.

Gordon, JA, Stryker, MP. 1996. Experience-Dependent Plasticity of Binocular Responses in the Primary Visual Cortex of the Mouse. J. Neurosci. 16: 3274–3286.

Greifzu, F, Schmidt, S, Schmidt, K-F, Kreikemeier, K, Witte, OW, Löwel, S. 2011. Global impairment and therapeutic restoration of visual plasticity mechanisms after a localized cortical stroke. Proc. Natl. Acad. Sci. 108: 15450–15455.

Guan, Z, Fang, J. 2006. Peripheral immune activation by lipopolysaccharide decreases neurotrophins in the cortex and hippocampus in rats. Brain. Behav. Immun. 20: 64–71.

Harlow, EG, Till, SM, Russell, TA, Wijetunge, LS, Kind, P, Contractor, A. 2010. Critical Period Plasticity Is Disrupted in the Barrel Cortex of Fmr1 Knockout Mice. Neuron 65: 385–398.

Hodos, RA, Kidd, BA, Shameer, K, Readhead, BP, Dudley, JT. 2016. In silico methods for drug repurposing and pharmacology. Wiley Interdiscip. Rev. Syst. Biol. Med. 8: 186–210.

Hong, F, Breitling, R, McEntee, CW, Wittner, BS, Nemhauser, JL, Chory, J. 2006. RankProd: a bioconductor package for detecting differentially expressed genes in meta-analysis. Bioinformatics 22: 2825–2827.

Huang, ZJ, Kirkwood, A, Pizzorusso, T, Porciatti, V, Morales, B, Bear, MF, Maffei, L, Tonegawa, S. 1999. BDNF Regulates the Maturation of Inhibition and the Critical Period of Plasticity in Mouse Visual Cortex. Cell 98: 739–755.

Jang, E, Lee, S, Kim, J-H, Kim, J-H, Seo, J-W, Lee, W-H, Mori, K, Nakao, K, Suk, K. 2013. Secreted protein lipocalin-2 promotes microglial M1 polarization. FASEB J. 27: 1176–1190.

Johnson, JS, Newport, EL. 1989. Critical period effects in second language learning: The influence of maturational state on the acquisition of English as a second language. Cognit. Psychol. 21: 60–99.

Kaneko, M, Stellwagen, D, Malenka, RC, Stryker, MP. 2008. Tumor Necrosis Factor-α Mediates One Component of Competitive, Experience-Dependent Plasticity in Developing Visual Cortex. Neuron 58: 673–680.

Khandaker GM, Pearson RM, Zammit S, Lewis G, Jones PB. 2014. Association of serum interleukin 6 and c-reactive protein in childhood with depression and psychosis in young adult life: A population-based longitudinal study. JAMA Psychiatry.

Knijnenburg, TA, Wessels, LFA, Reinders, MJT, Shmulevich, I. 2009. Fewer permutations, more accurate P-values. Bioinformatics 25: i161–i168.

Kuhlman, SJ, Olivas, ND, Tring, E, Ikrar, T, Xu, X, Trachtenberg, JT. 2013. A disinhibitory microcircuit initiates critical-period plasticity in the visual cortex. Nature 501: 543–546.

Layé, S, Parnet, P, Goujon, E, Dantzer, R. 1994. Peripheral administration of lipopolysaccharide induces the expression of cytokine transcripts in the brain and pituitary of mice. Mol. Brain Res. 27: 157–162.

LeBlanc, JJ, Fagiolini, M. 2011. Autism: A “Critical Period” Disorder? Neural Plast. 2011.

Lee, FS, Heimer, H, Giedd, JN, Lein, ES, Šestan, N, Weinberger, DR, Casey, BJ. 2014. Adolescent mental health—Opportunity and obligation. Science 346: 547–549.

Levelt, CN, Hübener, M. 2012. Critical-Period Plasticity in the Visual Cortex. Annu. Rev. Neurosci. 35: 309–330.

Lewis, TL, Maurer, D. 2005. Multiple sensitive periods in human visual development: evidence from visually deprived children. Dev. Psychobiol. 46: 163–183.

Marom, T, Tan, A, Wilkinson, GS, Pierson, KS, Freeman, JL, Chonmaitree, T. 2014. Trends in otitis media-related health care use in the United States, 2001-2011. JAMA Pediatr. 168: 68–75.

Mataga, N, Nagai, N, Hensch, TK. 2002. Permissive proteolytic activity for visual cortical plasticity. Proc. Natl. Acad. Sci. 99: 7717–7721.

Milnerwood, AJ, Cummings, DM, Dallérac, GM, Brown, JY, Vatsavayai, SC, Hirst, MC, Rezaie, P, Murphy, KPSJ. 2006. Early development of aberrant synaptic plasticity in a mouse model of Huntington's disease. Hum. Mol. Genet. 15: 1690–1703.

Miwa, JM, Stevens, TR, King, SL, Caldarone, BJ, Ibanez-Tallon, I, Xiao, C, Fitzsimonds, RM, Pavlides, C, Lester, HA, Picciotto, MR. 2006. The Prototoxin lynx1 Acts on Nicotinic Acetylcholine Receptors to Balance Neuronal Activity and Survival In Vivo. Neuron 51: 587–600.

Morishita, H, Hensch, TK. 2008. Critical period revisited: impact on vision. Curr. Opin. Neurobiol. 18: 101–107.

Morishita, H, Miwa, JM, Heintz, N, Hensch, TK. 2010. Lynx1, a Cholinergic Brake, Limits Plasticity in Adult Visual Cortex. Science 330: 1238–1240.

Murphy, KPSJ, Carter, RJ, Lione, LA, Mangiarini, L, Mahal, A, Bates, GP, Dunnett, SB, Morton, AJ. 2000. Abnormal Synaptic Plasticity and Impaired Spatial Cognition in Mice Transgenic for Exon 1 of the Human Huntington's Disease Mutation. J. Neurosci. 20: 5115–5123.

Nabel, EM, Morishita, H. 2013. Regulating Critical Period Plasticity: Insight from the Visual System to Fear Circuitry for Therapeutic Interventions. Front. Psychiatry 4.

Nagakura, I, Wart, AV, Petravicz, J, Tropea, D, Sur, M. 2014. STAT1 Regulates the Homeostatic Component of Visual Cortical Plasticity via an AMPA Receptor-Mediated Mechanism. J. Neurosci. 34: 10256–10263.

Nelson, CA, Zeanah, CH, Fox, NA, Marshall, PJ, Smyke, AT, Guthrie, D. 2007. Cognitive Recovery in Socially Deprived Young Children: The Bucharest Early Intervention Project. Science 318: 1937–1940.

Nikolopoulos, TP, O'Donoghue, GM, Archbold, S. 1999. Age at Implantation: Its Importance in Pediatric Cochlear Implantation. The Laryngoscope 109: 595–599.

Reh, R, Hensch, TK. 2014. Transient gamma power peaks upon monocular deprivation during critical period plasticity. In: 2014 Neuroscience Meeting Planner. Washington D.C.

Richwine, AF, Sparkman, NL, Dilger, RN, Buchanan, JB, Johnson, RW. 2009. Cognitive deficits in interleukin-10-deficient mice after peripheral injection of lipopolysaccharide. Brain. Behav. Immun. 23: 794–802.

Sayyah, M, Javad-Pour, M, Ghazi-Khansari, M. 2003. The bacterial endotoxin lipopolysaccharide enhances seizure susceptibility in mice: involvement of proinflammatory factors: nitric oxide and prostaglandins. Neuroscience 122: 1073–1080.

Schnydrig, S, Korner, L, Landweer, S, Ernst, B, Walker, G, Otten, U, Kunz, D. 2007. Peripheral lipopolysaccharide administration transiently affects expression of brain-derived neurotrophic factor, corticotropin and proopiomelanocortin in mouse brain. Neurosci. Lett. 429: 69–73.

Schorr, EA, Fox, NA, Wassenhove, V van, Knudsen, EI. 2005. Auditory-visual fusion in speech perception in children with cochlear implants. Proc. Natl. Acad. Sci. U. S. A. 102: 18748–18750.

Schroeter, M, Jander, S, Stoll, G. 2002. Non-invasive induction of focal cerebral ischemia in mice by photothrombosis of cortical microvessels: characterization of inflammatory responses. J. Neurosci. Methods 117: 43–49.

Sipe, GO, Lowery, undefined RL, Tremblay, M-È, Kelly, EA, Lamantia, CE, Majewska, AK. 2016. Microglial P2Y12 is necessary for synaptic plasticity in mouse visual cortex. Nat. Commun. 7: 10905.

Smyth, GK. 2005. Limma: linear models for microarray data. In: Bioinformatics and Computational Biology Solutions using R and Bioconductor. New York: Springer, p 397–420.

Steullet, P, Cabungcal, JH, Monin, A, Dwir, D, O'Donnell, P, Cuenod, M, Do, KQ. 2014. Redox dysregulation, neuroinflammation, and NMDA receptor hypofunction: A "central hub" in schizophrenia pathophysiology? Schizophr. Res.

Subramanian, A, Tamayo, P, Mootha, VK, Mukherjee, S, Ebert, BL, Gillette, MA, Paulovich, A, Pomeroy, SL, Golub, TR, Lander, ES, Mesirov, JP. 2005. Gene set enrichment analysis: A knowledge-based approach for interpreting genome-wide expression profiles. Proc. Natl. Acad. Sci. 102: 15545–15550.

Syken, J, GrandPre, T, Kanold, PO, Shatz, CJ. 2006. PirB Restricts Ocular-Dominance Plasticity in Visual Cortex. Science 313: 1795–1800.

Takesian, AE, Hensch, TK. 2013. Chapter 1 - Balancing Plasticity/Stability Across Brain Development. In: Michael M. Merzenich, MN and TMVV, editor. Progress in Brain Research Changing BrainsApplying Brain Plasticity to Advance and Recover Human Ability. Elsevier, p 3–34.

Tropea, D, Giacometti, E, Wilson, NR, Beard, C, McCurry, C, Fu, DD, Flannery, R, Jaenisch, R, Sur, M. 2009. Partial reversal of Rett Syndrome-like symptoms in MeCP2 mutant mice. Proc. Natl. Acad. Sci. 106: 2029–2034.

Usdin, MT, Shelbourne, PF, Myers, RM, Madison, DV. 1999. Impaired Synaptic Plasticity in Mice Carrying the Huntington’s Disease Mutation. Hum. Mol. Genet. 8: 839–846.

Vezzani, A, Granata, T. 2005. Brain Inflammation in Epilepsy: Experimental and Clinical Evidence. Epilepsia 46: 1724–1743.

Wang, B-S, Sarnaik, R, Cang, J. 2010. Critical Period Plasticity Matches Binocular Orientation Preference in the Visual Cortex. Neuron 65: 246–256.

Weber-Stadlbauer, U, Richetto, J, Labouesse, MA, Bohacek, J, Mansuy, IM, Meyer, U. 2016. Transgenerational transmission and modification of pathological traits induced by prenatal immune activation. Mol. Psychiatry.

Weinberger DR. 1987. Implications of normal brain development for the pathogenesis of schizophrenia. Arch. Gen. Psychiatry 44: 660–669.

Werker, JF, Hensch, TK. 2015. Critical Periods in Speech Perception: New Directions. Annu. Rev. Psychol. 66: 173–196.

Wiesel, TN, Hubel, DH. 1963. Single-Cell Responses in Striate Cortex of Kittens Deprived of Vision in One Eye. J. Neurophysiol. 26: 1003–1017.

Yashiro, K, Riday, TT, Condon, KH, Roberts, AC, Bernardo, DR, Prakash, R, Weinberg, RJ, Ehlers, MD, Philpot, BD. 2009. Ube3a is required for experience-dependent maturation of the neocortex. Nat. Neurosci. 12: 777–783.

Zhang, S-D, Gant, TW. 2008. A simple and robust method for connecting small-molecule drugs using gene-expression signatures. BMC Bioinformatics 9: 258.

LEGENDS

Figure 1: Diseases that dysregulate the juvenile plasticity signature are associated with inflammatory processes. **(a)** Juvenile plasticity signature of 176 genes (represented by green bars) generated by differential expression of P29 vs >P60 C57Bl6 male mice primary visual cortex was computationally matched to 436 disease signatures (represented by orange bars) using **(b)** rank-based molecular matching where large scores indicate shared transcriptional phenotype. **(c)** Disease Leverage Analysis (DLA) systematically identified processes associated to diseases that dysregulate the plasticity signature. 7 of 14 largest associations were inflammation-related gene sets and 7 of 7 of inflammation-related gene sets were strongly associated to plasticity (all at $p_{corrected} < 5 \times 10^{-5}$: OR = 25.8, 95% CI = [1.4, 491.2], $p = 2.7 \times 10^{-3}$, Fisher's Exact Test). See Figure 1-1 for source DLA data.

Figure 1-1: Disease Leverage Analysis (DLA) identifies biological processes common to diseases that perturb the juvenile plasticity signature. To identify shared pathophysiology across the diverse list of diseases predicted to dysregulate the juvenile plasticity signature, we applied DLA. This approach calculates the association between diseases that dysregulate the plasticity signature genes and 50 well-defined and distinct biological pathways. To do so, it computes a regression between the molecular match score (a measure that indicates the strength of association between the disease and plasticity signatures; see Table 2 and Materials and Methods) and the pathology score (a measure of activity of the biological pathway in that disease; see Materials and Methods). Large regression coefficients indicate that the biological pathway may disrupt juvenile plasticity. Using a multiple-test corrected, empirical $p < 5 \times 10^{-5}$, 7 of 14 largest DLA associations were inflammation-related gene sets and every inflammation-related gene set in the hallmark library was strongly associated with diseases that dysregulate plasticity genes (7/7 inflammation gene sets at $p_{corrected} < 5 \times 10^{-5}$: OR = 25.8, 95% CI = [1.4, 491.2], $p = 2.7 \times 10^{-3}$, Fisher's Exact Test). 20,000 permutations of the gene sets were used to estimate p-values and to normalize the regression coefficients to allow comparison between effect sizes for different biological pathways. Inflammation-related gene sets: TNFa Signaling via NFKb, Interferon Gamma Response, Inflammatory Response, Complement, Il2-Stat5 Signaling, Interferon Alpha response, Il6-Jak-Stat3 Signaling.

Figure 2: Diseases that dysregulate the adult Lynx1$^{-/-}$ plasticity signature are associated with inflammatory processes. Using an adult Lynx1$^{-/-}$ plasticity signature of 98 genes (generated by differential expression of primary visual cortex from >P60 Lynx1$^{-/-}$ vs >P60 C57Bl6 male mice), Disease Leverage Analysis (DLA) systematically identified biological processes associated to diseases that dysregulate the adult Lynx1$^{-/-}$ plasticity signature genes. Using adult Lynx1$^{-/-}$ animals controls for age, as these adult animals have elevated plasticity similar to juvenile animals. 7 of 11 largest associations were inflammation-related gene sets and every inflammation-related gene set was strongly associated to plasticity (7/7 inflammation gene sets at $p_{corrected} < 5 \times 10^{-5}$: OR = 63.0, 95% CI = [3.2, 1,229.8], $p = 7.6 \times 10^{-5}$, Fisher's Exact Test). See Figure 2-1 for source DLA data.

Figure 2-1: Disease Leverage Analysis (DLA) identifies biological processes common to diseases that perturb the Lynx1$^{-/-}$ plasticity signature. To identify shared pathophysiology across the diverse list of diseases predicted to dysregulate the Lynx1$^{-/-}$ plasticity signature, we applied DLA. Large regression coefficients indicate that the biological pathway may disrupt Lynx1$^{-/-}$ plasticity. As with the juvenile plasticity signature, using a multiple-test corrected, empirical $p < 5 \times 10^{-5}$, we found that every inflammation-related gene set in the hallmark library was strongly associated with diseases that dysregulate plasticity genes (7/7 inflammation gene sets at $p_{corrected} < 5 \times 10^{-5}$: OR = 63.0, 95% CI = [3.2, 1,229.8], $p = 7.6 \times 10^{-5}$ Fisher's Exact Test). 20,000 permutations of the gene sets were used to estimate p-values and to normalize the regression coefficients to allow comparison between effect sizes for different biological pathways. Inflammation-related gene sets: TNFa Signaling via NFKb, Interferon Gamma Response, Inflammatory Response, Complement, Il2-Stat5 Signaling, Interferon Alpha response, Il6-Jak-Stat3 Signaling.

Figure 3: Lipopolysaccharide (LPS) reverses plasticity signature gene expression. (a) LPS disease signature shares plasticity signature genes *in silico* (Molecular match rank #14, $p = 7.9 \times 10^{-4}$; see Table 2; disease signature is from GSE3253: adult mouse whole brain homogenate harvested 4h after peripheral LPS injected i.p.; genes with absolute value of the standardized expression (Z-score) greater than or equal to 2 standard deviations from the mean were selected as the most differentially expressed by LPS). **(b)** The expression of the 16 genes shared between juvenile plasticity and the LPS disease signatures is anti-correlated (Spearman's ρ = -0.77, $p = 7.4 \times 10^{-4}$; LPS disease signature gene expression values fell in the range [-1,+1]; For plotting purposes, plasticity gene expression fold

change was linear transformed to [-1,+1]). **(c)** Of 13 genes out of 16 predicted to be reversed by LPS, the majority (8/13; 61.5%) showed a complete reversal in their differential expression pattern in primary visual cortex (V1) after LPS administration (300 μg/Kg LPS injected i.p. at P26 during the peak of juvenile plasticity) relative to saline. LPS downregulated Cldn5 and Slc40a1 and upregulated Alox12b, S100a9a, Ch25h, Lrg1, S100a8, Lcn2, (n = 5 mice per group). *** $p < 0.001$, ** $0.001 < p \leq 0.01$, * $0.01 < p \leq 0.05$ (two-sided t-tests of ΔCTs). Log2 fold change is -$\Delta\Delta$CT. Error bars, SEM.

Figure 4: Inflammation induced by lipopolysaccharide (LPS) suppresses experience-dependent plasticity in juvenile cortex. (a) Juvenile mice (P26) during the peak of ocular dominance plasticity were injected i.p. with either LPS (300 μg/Kg) or saline. Mice were either (b) subjected to qPCR analysis of plasticity effectors from primary visual cortex (V1) 4h after the injection or (c) underwent 3 days of monocular deprivation (MD) followed by *in vivo* extracellular recordings to assess ocular dominance plasticity. **(b)** LPS increased known plasticity brakes Pirb and H2K1 & H2K1, and decreased the plasticity trigger BDNF. LPS had no effect on the plasticity effectors Nptx2, Lynx1, NogoR, or Ppp3ca. Log2 FC (fold change) is -$\Delta\Delta$CT (n = 5 mice per group). Error bar: SEM. *** $p < 0.001$, ** $0.001 < p \leq 0.01$, * $0.01 < p \leq 0.05$ (*t*-test of ΔCTs). **(c)** Neurons from peripheral LPS-treated mice (purple histogram: n = 7 mice, 129 cells) showed decreased cortical responsivity to light in the ipsilateral versus contralateral eye, as quantified by a reduced right shift in the ocular dominance score (ODS) distribution after 3 days of MD compared to control saline-treated juvenile mice with MD (gray histogram: 6 mice, 135 cells: χ^2 test of ODS distribution: $p = 2.6 \times 10^{-06}$). Animal-level quantification of ocular dominance

plasticity by contralateral bias index (CBI) reflects the extent of ocular dominance shift after 3 days of MD (right side plot; low CBI indicates higher plasticity). CBI was strongly increased in LPS-treated group (purple discs: CBI=0.64 ± 0.02, 7 mice) compared to saline-treated group (grey discs: CBI = 0.49 ± 0.04, 6 mice), indicating that pro-inflammatory LPS had suppressed developmental plasticity (LPS vs saline, ** $p = 6 \times 10^{-3}$, one-sided *t*-test). qPCR data are mean ± SEM. Horizontal bars for CBI plot = mean.

Table 1: Juvenile plasticity signature. Primary visual cortex (V1) transcriptomes were profiled with microarray from juvenile mice with naturally elevated experience-dependent plasticity to generate the juvenile plasticity differential expression signature. Using RankProd differential expression (DE) analysis, V1 of juvenile male mice C57Bl6 at postnatal day 29 (P29) was compared to adult C57Bl6 mice (> P60) (n = 3 each group) to identify 248 DE probes, which mapped to 193 unique mouse Entrez IDs. For downstream analysis, mouse Entrez IDs were mapped to human orthologues using the Mouse Genome Informatics homology reference to yield a 176 gene juvenile plasticity signature.

Table 2: Molecular matching between 436 disease signatures and the juvenile plasticity signature indicates diverse diseases may disrupt plasticity. We computationally matched the juvenile plasticity signature to 436 disease signatures derived from public microarray data. This systematic method applies a rank-based molecular matching algorithm to determine the molecular concordance between the plasticity signature and a given disease signature, where high scores indicate plasticity genes are significantly dysregulated by the disease and low scores indicate that the disease

has no impact on plasticity genes. Highly ranked diseases included not only brain disorders known to disrupt plasticity such as Huntington's Disease, but also non-neurologic disorders (e.g. bacterial infections, inflammatory bowel disease, metabolic diseases), suggesting a broad range of disease states may impact molecular pathways involved in plasticity.

Table 3: Lynx1$^{-/-}$ plasticity signature. Primary visual cortex (V1) transcriptomes were profiled with microarray from Lynx1$^{-/-}$ mice (the plasticity brake Lynx1 is genetically deleted to allow experience-dependent plasticity even in adulthood) to generate the Lynx1$^{-/-}$ plasticity differential expression signature. Using RankProd differential expression (DE) analysis, V1 of adult Lynx1$^{-/-}$ male mice older than postnatal day 60 (>P60) was compared to adult wild-type mice (> P60) (n = 3 each group) to identify 132 DE probes, which mapped to 107 unique mouse Entrez IDs. For downstream analysis, mouse Entrez IDs were mapped to human orthologues using the Mouse Genome Informatics homology reference to yield a 98 gene Lynx1$^{-/-}$ plasticity signature.

TABLES, FIGURES, AND MULTIMEDIA

Tables and figures and data sources have been uploaded separately.

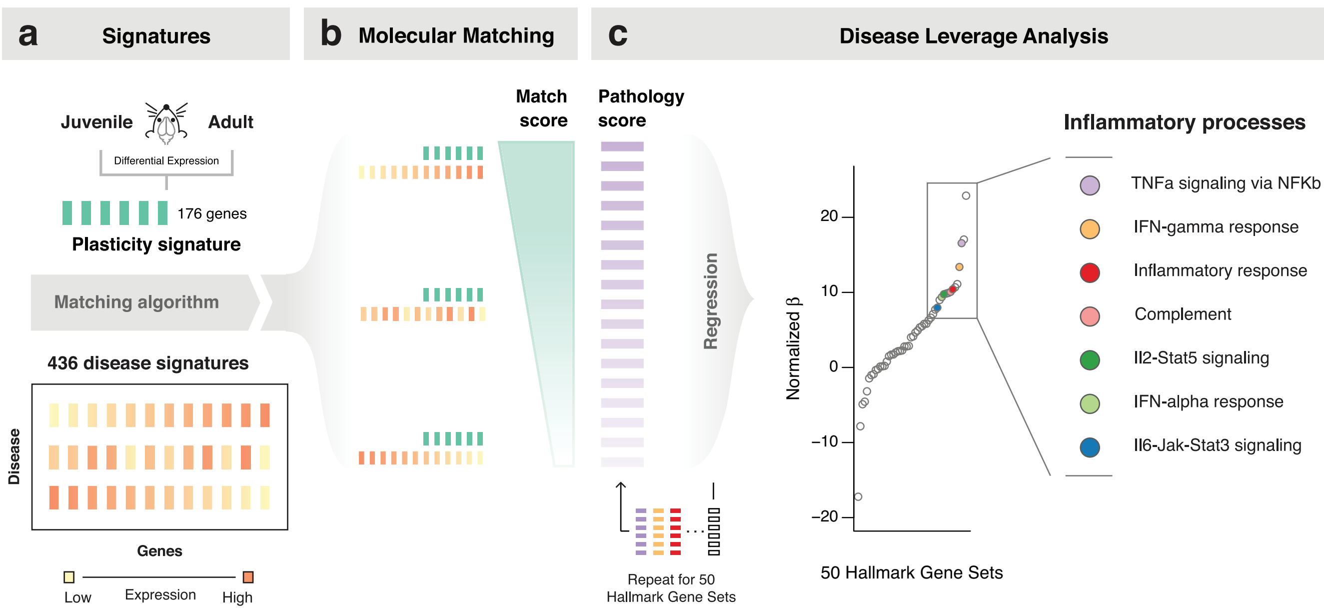
a
Signatures
Juvenile
Adult
Differential Expression
176 genes
Plasticity signature
Matching algorithm
436 disease signatures
Disease
Genes
Low
Expression
High
b
Molecular Matching
Match score
c
Disease Leverage Analysis
Pathology score
Regression
Repeat for 50 Hallmark Gene Sets
Normalized β
20
10
0
−10
−20
50 Hallmark Gene Sets
Inflammatory processes
TNFa signaling via NFKb
IFN-gamma response
Inflammatory response
Complement
Il2-Stat5 signaling
IFN-alpha response
Il6-Jak-Stat3 signaling

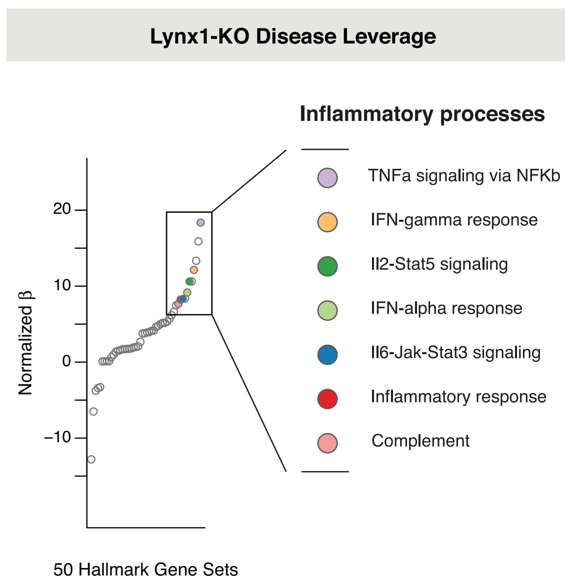

Lynx1-KO Disease Leverage
Inflammatory processes
TNFa signaling via NFKb
IFN-gamma response
Il2-Stat5 signaling
IFN-alpha response
Il6-Jak-Stat3 signaling
Inflammatory response
Complement
20
10
0
−10
Normalized β
50 Hallmark Gene Sets

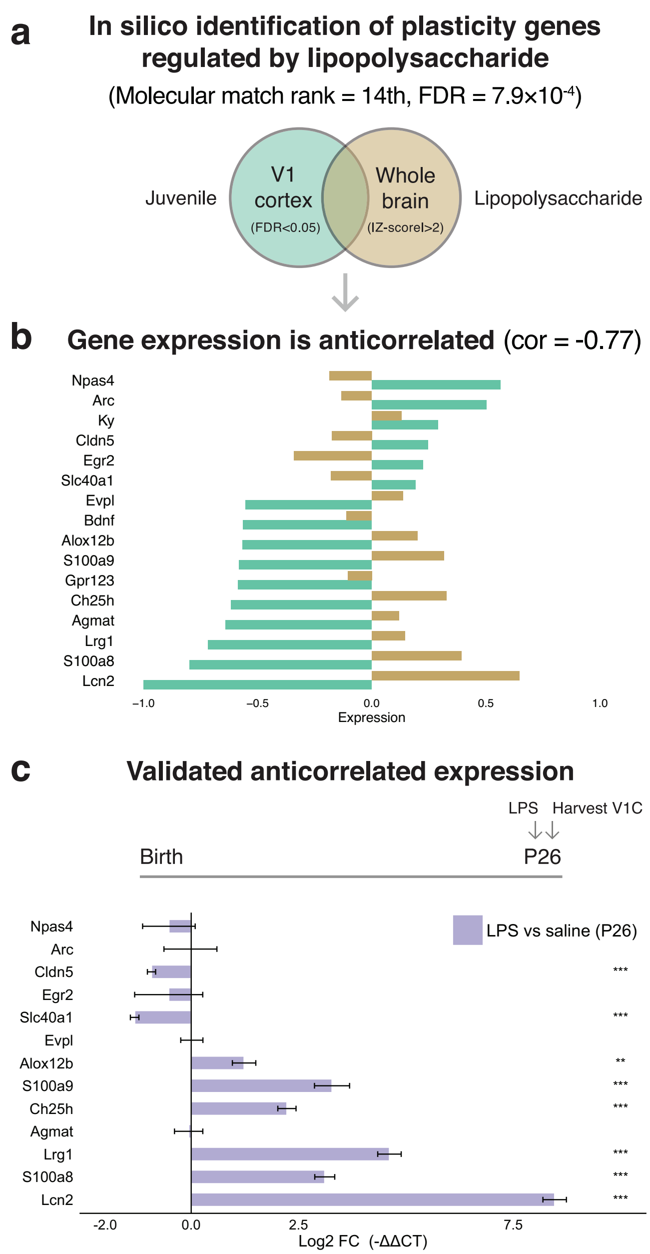
a
In silico identification of plasticity genes regulated by lipopolysaccharide
(Molecular match rank = 14th, FDR = 7.9×10⁻⁴)
Juvenile
V1 cortex
(FDR<0.05)
Whole brain
(|Z-score|>2)
Lipopolysaccharide
b
Gene expression is anticorrelated (cor = -0.77)
Npas4
Arc
Ky
Cldn5
Egr2
Slc40a1
Evpl
Bdnf
Alox12b
S100a9
Gpr123
Ch25h
Agmat
Lrg1
S100a8
Lcn2
−1.0
−0.5
0.0
0.5
1.0
Expression
c
Validated anticorrelated expression
LPS
Harvest V1C
Birth
P26
LPS vs saline (P26)
Npas4
Arc
Cldn5
Egr2
Slc40a1
Evpl
Alox12b
S100a9
Ch25h
Agmat
Lrg1
S100a8
Lcn2
***
***
**
***
***
***
***
***
-2.0
0.0
2.5
7.5
Log2 FC (-ΔΔCT)

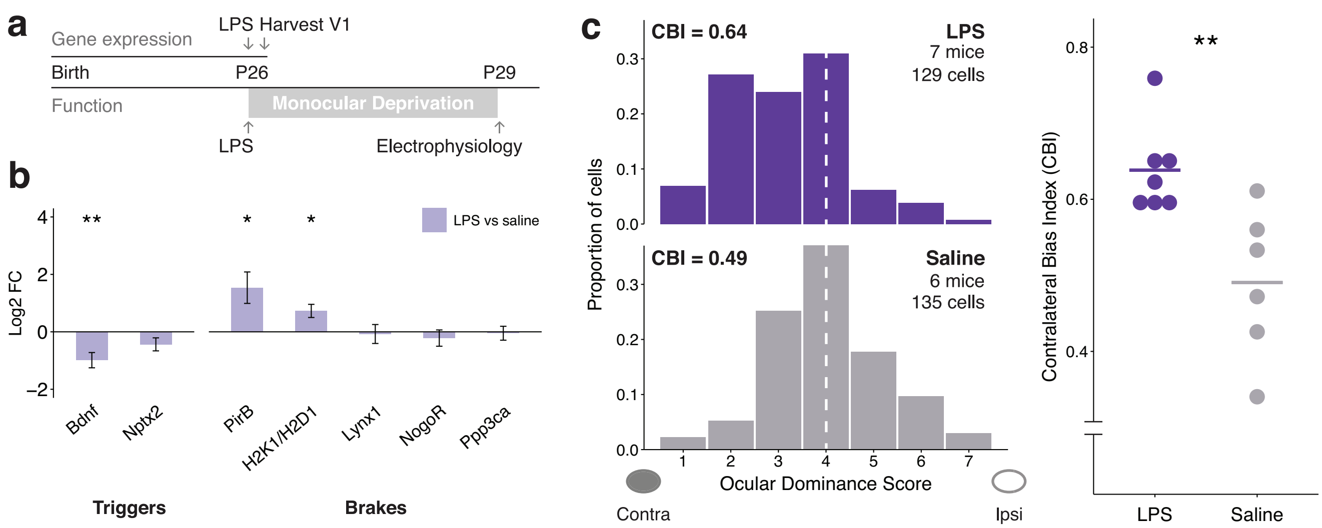
a
Gene expression
LPS Harvest V1
Birth
P26
P29
Function
Monocular Deprivation
LPS
Electrophysiology
b
LPS vs saline
Log2 FC
Bdnf
Nptx2
PirB
H2K1/H2D1
Lynx1
NogoR
Ppp3ca
Triggers
Brakes
c
CBI = 0.64
LPS
7 mice
129 cells
CBI = 0.49
Saline
6 mice
135 cells
Proportion of cells
Ocular Dominance Score
Contra
Ipsi
Contralateral Bias Index (CBI)
LPS
Saline

Figure 1-1 (Source data for Figure 1). Disease Leverage Analysis (DLA) identifies biological processes common to diseases that perturb the juvenile plasticity signature.

	Name	Normalized_effect	Betas	Pval	Bonferroni
HALLMARK_EPITHELIAL_MESENCHYMAL_TRANSITION	epithelial mesenchymal transition	22.89	7.44	5.7E-15	2.8E-13
HALLMARK_KRAS_SIGNALING_UP	kras signaling up	17.05	5.49	0.0E+00	0.0E+00
HALLMARK_TNFA_SIGNALING_VIA_NFKB	**tnfa signaling via nfkb**	**16.57**	**5.35**	**6.0E-13**	**3.0E-11**
HALLMARK_INTERFERON_GAMMA_RESPONSE	**interferon gamma response**	**13.40**	**4.33**	**5.3E-18**	**2.6E-16**
HALLMARK_HYPOXIA	hypoxia	11.11	3.52	3.9E-10	2.0E-08
HALLMARK_ESTROGEN_RESPONSE_LATE	estrogen response late	10.68	3.39	6.8E-10	3.4E-08
HALLMARK_INFLAMMATORY_RESPONSE	**inflammatory response**	**10.42**	**3.33**	**1.4E-14**	**6.8E-13**
HALLMARK_COMPLEMENT	**complement**	**10.08**	**3.18**	**0.0E+00**	**0.0E+00**
HALLMARK_E2F_TARGETS	e2f targets	9.94	3.14	2.2E-09	1.1E-07
HALLMARK_ANGIOGENESIS	angiogenesis	9.85	1.39	3.2E-07	1.6E-05
HALLMARK_IL2_STAT5_SIGNALING	**il2 stat5 signaling**	**9.78**	**3.09**	**2.8E-09**	**1.4E-07**
HALLMARK_INTERFERON_ALPHA_RESPONSE	**interferon alpha response**	**9.38**	**2.09**	**4.6E-12**	**2.3E-10**
HALLMARK_G2M_CHECKPOINT	g2m checkpoint	9.00	2.85	2.2E-12	1.1E-10
HALLMARK_IL6_JAK_STAT3_SIGNALING	**il6 jak stat3 signaling**	**7.98**	**1.70**	**2.6E-09**	**1.3E-07**
HALLMARK_ESTROGEN_RESPONSE_EARLY	estrogen response early	7.72	2.40	1.2E-07	6.0E-06
HALLMARK_UV_RESPONSE_DN	uv response dn	7.11	1.90	3.1E-11	1.6E-09
HALLMARK_ALLOGRAFT_REJECTION	allograft rejection	6.63	2.04	4.1E-09	2.1E-07
HALLMARK_TGF_BETA_SIGNALING	tgf beta signaling	6.30	1.06	1.1E-06	5.5E-05
HALLMARK_COAGULATION	coagulation	5.82	1.51	6.3E-07	3.2E-05
HALLMARK_APOPTOSIS	apoptosis	5.81	1.62	8.2E-07	4.1E-05
HALLMARK_APICAL_JUNCTION	apical junction	5.50	1.66	1.0E-06	5.2E-05
HALLMARK_MYOGENESIS	myogenesis	5.33	1.61	2.3E-06	1.1E-04
HALLMARK_P53_PATHWAY	p53 pathway	4.93	1.47	9.8E-05	4.9E-03
HALLMARK_CHOLESTEROL_HOMEOSTASIS	cholesterol homeostasis	4.66	0.89	6.8E-05	3.4E-03
HALLMARK_XENOBIOTIC_METABOLISM	xenobiotic metabolism	4.14	1.21	1.3E-03	6.3E-02
HALLMARK_UV_RESPONSE_UP	uv response up	4.02	1.06	6.5E-04	3.3E-02
HALLMARK_MTORC1_SIGNALING	mtorc1 signaling	2.87	0.79	3.3E-02	1.0E+00
HALLMARK_MITOTIC_SPINDLE	mitotic spindle	2.81	0.76	3.5E-02	1.0E+00

HALLMARK_GLYCOLYSIS	glycolysis	2.80	0.77	3.8E-02	1.0E+00
HALLMARK_ANDROGEN_RESPONSE	androgen response	2.27	0.45	7.4E-02	1.0E+00
HALLMARK_KRAS_SIGNALING_DN	kras signaling dn	2.21	0.56	1.3E-01	1.0E+00
HALLMARK_BILE_ACID_METABOLISM	bile acid metabolism	2.16	0.44	1.0E-01	1.0E+00
HALLMARK_HEDGEHOG_SIGNALING	hedgehog signaling	1.99	0.25	8.2E-02	1.0E+00
HALLMARK_PANCREAS_BETA_CELLS	pancreas beta cells	1.73	0.22	1.5E-01	1.0E+00
HALLMARK_WNT_BETA_CATENIN_SIGNALING	wnt beta catenin signaling	1.71	0.23	1.5E-01	1.0E+00
HALLMARK_NOTCH_SIGNALING	notch signaling	1.50	0.17	2.1E-01	1.0E+00
HALLMARK_APICAL_SURFACE	apical surface	0.79	0.09	6.0E-01	1.0E+00
HALLMARK_UNFOLDED_PROTEIN_RESPONSE	unfolded protein response	0.21	-0.04	8.8E-01	1.0E+00
HALLMARK_MYC_TARGETS_V2	myc targets v2	0.15	-0.02	9.1E-01	1.0E+00
HALLMARK_PEROXISOME	peroxisome	0.13	-0.06	8.3E-01	1.0E+00
HALLMARK_FATTY_ACID_METABOLISM	fatty acid metabolism	-0.21	-0.20	5.6E-01	1.0E+00
HALLMARK_SPERMATOGENESIS	spermatogenesis	-0.34	-0.21	4.9E-01	1.0E+00
HALLMARK_ADIPOGENESIS	adipogenesis	-0.90	-0.47	2.1E-01	1.0E+00
HALLMARK_REACTIVE_OXIGEN_SPECIES_PATHWAY	reactive oxigen species pathway	-1.02	-0.21	2.2E-01	1.0E+00
HALLMARK_PI3K_AKT_MTOR_SIGNALING	pi3k akt mtor signaling	-1.45	-0.45	8.7E-02	1.0E+00
HALLMARK_HEME_METABOLISM	heme metabolism	-3.18	-1.24	2.0E-04	1.0E-02
HALLMARK_PROTEIN_SECRETION	protein secretion	-4.56	-1.15	0.0E+00	0.0E+00
HALLMARK_DNA_REPAIR	dna repair	-4.90	-1.52	0.0E+00	0.0E+00
HALLMARK_MYC_TARGETS_V1	myc targets v1	-7.83	-2.78	0.0E+00	0.0E+00
HALLMARK_OXIDATIVE_PHOSPHORYLATION	oxidative phosphorylation	-17.22	-5.92	0.0E+00	0.0E+00

Figure 2-1 (Source data for Figure 2). Disease Leverage Analysis (DLA) identifies biological processes common to diseases that perturb the Lynx1-/- plasticity signature.

	Name	Normalized_effect	Betas	Pval	Bonferroni
HALLMARK_TNFA_SIGNALING_VIA_NFKB	**tnfa signaling via nfkb**	**18.38**	**6.60**	**0.0E+00**	**0.0E+00**
HALLMARK_EPITHELIAL_MESENCHYMAL_TRANSITION	epithelial mesenchymal transition	15.90	5.66	2.6E-17	1.3E-15
HALLMARK_KRAS_SIGNALING_UP	kras signaling up	13.34	4.70	0.0E+00	0.0E+00
HALLMARK_INTERFERON_GAMMA_RESPONSE	**interferon gamma response**	**12.15**	**4.28**	**6.1E-13**	**3.1E-11**
HALLMARK_HYPOXIA	hypoxia	10.62	3.65	5.6E-12	2.8E-10
HALLMARK_IL2_STAT5_SIGNALING	**il2 stat5 signaling**	**10.62**	**3.65**	**1.4E-12**	**7.1E-11**
HALLMARK_INTERFERON_ALPHA_RESPONSE	**interferon alpha response**	**9.17**	**2.23**	**4.9E-11**	**2.4E-09**
HALLMARK_ANGIOGENESIS	angiogenesis	8.38	1.32	4.5E-07	2.2E-05
HALLMARK_IL6_JAK_STAT3_SIGNALING	**il6 jak stat3 signaling**	**8.32**	**1.95**	**1.3E-09**	**6.5E-08**
HALLMARK_INFLAMMATORY_RESPONSE	**inflammatory response**	**8.24**	**2.78**	**1.9E-08**	**9.7E-07**
HALLMARK_COMPLEMENT	**complement**	**7.67**	**2.54**	**7.7E-09**	**3.9E-07**
HALLMARK_ESTROGEN_RESPONSE_LATE	estrogen response late	7.49	2.46	7.7E-08	3.8E-06
HALLMARK_TGF_BETA_SIGNALING	tgf beta signaling	6.63	1.22	1.7E-07	8.7E-06
HALLMARK_APOPTOSIS	apoptosis	6.17	1.82	5.8E-07	2.9E-05
HALLMARK_ALLOGRAFT_REJECTION	allograft rejection	5.71	1.80	5.6E-05	2.8E-03
HALLMARK_ESTROGEN_RESPONSE_EARLY	estrogen response early	5.33	1.64	3.1E-04	1.5E-02
HALLMARK_CHOLESTEROL_HOMEOSTASIS	cholesterol homeostasis	5.17	1.07	8.8E-05	4.4E-03
HALLMARK_COAGULATION	coagulation	5.17	1.38	1.8E-04	9.1E-03
HALLMARK_P53_PATHWAY	p53 pathway	5.02	1.52	9.5E-04	4.8E-02
HALLMARK_MYOGENESIS	myogenesis	4.78	1.44	2.3E-03	1.2E-01
HALLMARK_G2M_CHECKPOINT	g2m checkpoint	4.63	1.38	3.3E-03	1.7E-01
HALLMARK_APICAL_JUNCTION	apical junction	4.16	1.21	1.4E-02	7.1E-01
HALLMARK_E2F_TARGETS	e2f targets	4.13	1.18	1.6E-02	8.2E-01
HALLMARK_MTORC1_SIGNALING	mtorc1 signaling	3.95	1.13	2.4E-02	1.0E+00
HALLMARK_UV_RESPONSE_UP	uv response up	3.90	1.03	1.3E-02	6.5E-01
HALLMARK_XENOBIOTIC_METABOLISM	xenobiotic metabolism	3.81	1.06	3.7E-02	1.0E+00
HALLMARK_UV_RESPONSE_DN	uv response dn	3.77	0.96	1.7E-02	8.3E-01
HALLMARK_BILE_ACID_METABOLISM	bile acid metabolism	2.68	0.55	1.3E-01	1.0E+00
HALLMARK_GLYCOLYSIS	glycolysis	2.08	0.41	5.0E-01	1.0E+00
HALLMARK_FATTY_ACID_METABOLISM	fatty acid metabolism	1.99	0.38	4.5E-01	1.0E+00
HALLMARK_SPERMATOGENESIS	spermatogenesis	1.95	0.36	4.2E-01	1.0E+00

HALLMARK_WNT_BETA_CATENIN_SIGNALING	wnt beta catenin signaling	1.81	0.24	2.2E-01	1.0E+00
HALLMARK_ADIPOGENESIS	adipogenesis	1.76	0.29	6.4E-01	1.0E+00
HALLMARK_HEDGEHOG_SIGNALING	hedgehog signaling	1.74	0.21	2.3E-01	1.0E+00
HALLMARK_ANDROGEN_RESPONSE	androgen response	1.72	0.27	4.5E-01	1.0E+00
HALLMARK_PEROXISOME	peroxisome	1.70	0.28	4.5E-01	1.0E+00
HALLMARK_NOTCH_SIGNALING	notch signaling	1.59	0.18	2.8E-01	1.0E+00
HALLMARK_PANCREAS_BETA_CELLS	pancreas beta cells	1.50	0.18	3.5E-01	1.0E+00
HALLMARK_KRAS_SIGNALING_DN	kras signaling dn	1.37	0.14	8.2E-01	1.0E+00
HALLMARK_MITOTIC_SPINDLE	mitotic spindle	0.98	-0.01	9.8E-01	1.0E+00
HALLMARK_UNFOLDED_PROTEIN_RESPONSE	unfolded protein response	0.64	-0.03	9.4E-01	1.0E+00
HALLMARK_MYC_TARGETS_V2	myc targets v2	0.12	-0.09	7.3E-01	1.0E+00
HALLMARK_REACTIVE_OXIGEN_SPECIES_PATHWAY	reactive oxigen species pathway	0.12	-0.07	7.5E-01	1.0E+00
HALLMARK_PI3K_AKT_MTOR_SIGNALING	pi3k akt mtor signaling	0.11	-0.17	6.5E-01	1.0E+00
HALLMARK_APICAL_SURFACE	apical surface	0.10	-0.07	7.5E-01	1.0E+00
HALLMARK_PROTEIN_SECRETION	protein secretion	-3.28	-1.07	3.5E-04	1.8E-02
HALLMARK_HEME_METABOLISM	heme metabolism	-3.41	-1.69	2.5E-04	1.3E-02
HALLMARK_DNA_REPAIR	dna repair	-3.77	-1.51	0.0E+00	0.0E+00
HALLMARK_MYC_TARGETS_V1	myc targets v1	-6.49	-2.86	0.0E+00	0.0E+00
HALLMARK_OXIDATIVE_PHOSPHORYLATION	oxidative phosphorylation	-12.79	-5.25	0.0E+00	0.0E+00

Table 1. Juvenile plasticity signature.

RP	FC	pfp	pvalue	probe_id	symbol	mm_entrez_id	hs_entrez_id	gene_name
2.8187	3.7313	0	0	ILMN_2641456	Pcp2	18545	126006	Purkinje cell protein 2 (L7)
3.2916	3.422	0	0	ILMN_2503052	Tnnc1	21924	7134	troponin C, cardiac/slow skeletal
4.2819	3.1519	0	0	ILMN_2794645	Cyr61	16007	3491	cysteine rich protein 61
13.632	2.5389	0	0	ILMN_1251414	Npas4	225872	266743	neuronal PAS domain protein 4
28.3181	2.375	0	0	ILMN_2597827	Arc	11838	23237	activity regulated cytoskeletal-associated protein
15.7472	2.3415	0	0	ILMN_1230397	A630064P09Rik	NA	NA	NA
15.7373	2.331	0	0	ILMN_2622983	Dusp1	19252	1843	dual specificity phosphatase 1
14.4292	2.3046	0	0	ILMN_3160970	Gpr17	574402	2840	G protein-coupled receptor 17
16.9658	2.2123	0	0	ILMN_1250438	Marcksl1	17357	65108	MARCKS-like 1
21.67	2.1606	0	0	ILMN_2710253	Cyr61	16007	3491	cysteine rich protein 61
20.9478	2.1439	0	0	ILMN_1217458	8430403J19Rik	NA	NA	NA
23.8738	2.111	0	0	ILMN_1220034	Junb	16477	3726	jun B proto-oncogene
27.1365	2.0864	0	0	ILMN_2744890	Gadd45g	23882	10912	growth arrest and DNA-damage-inducible 45 gamma
25.9586	2.0549	0	0	ILMN_1227299	Mbp	17196	4155	myelin basic protein
29.3188	2.0001	0	0	ILMN_1239557	Ugt8a	22239	7368	UDP galactosyltransferase 8A
27.0514	1.9972	0	0	ILMN_2619767	Pdlim2	213019	64236	PDZ and LIM domain 2
32.1696	1.9948	0	0	ILMN_2707616	Col22a1	69700	169044	collagen, type XXII, alpha 1
32.3997	1.9656	0	0	ILMN_1221178	Pdlim2	213019	64236	PDZ and LIM domain 2
38.5983	1.9267	5.00E-04	0	ILMN_2463181	Tnc	21923	3371	tenascin C
37.2206	1.9239	5.00E-04	0	ILMN_2810882	Ppic	19038	5480	peptidylprolyl isomerase C
41.0256	1.9217	5.00E-04	0	ILMN_2615034	Mog	17441	4340	myelin oligodendrocyte glycoprotein
37.2906	1.9117	5.00E-04	0	ILMN_2653205	Gp1bb	14724	2812	glycoprotein Ib, beta polypeptide
43.0584	1.9067	4.00E-04	0	ILMN_1212702	Hba-a1	NA	NA	NA
47.3908	1.8855	8.00E-04	0	ILMN_1240973	Slc29a4	243328	222962	solute carrier family 29 (nucleoside transporters), member 4
145.4493	1.8339	0.0108	0	ILMN_1253365	Lypd1	71111	2863	G protein-coupled receptor 39
49.1546	1.832	8.00E-04	0	ILMN_2802263	Cnp	12799	1267	2',3'-cyclic nucleotide 3' phosphodiesterase
89.4321	1.8212	0.0037	0	ILMN_2491182	A130010C12Rik	NA	NA	NA
85.0435	1.8206	0.0024	0	ILMN_2766894	Enpp6	320981	133121	ectonucleotide pyrophosphatase/phosphodiesterase 6
60.0087	1.7971	8.00E-04	0	ILMN_1223244	Hbb-b1	NA	NA	NA
71.2786	1.7908	0.0012	0	ILMN_2906855	Ky	16716	339855	kyphoscoliosis peptidase

63.327	1.7828	7.00E-04	0	ILMN_2880906	Pdlim2	213019	64236	PDZ and LIM domain 2
79.6764	1.7799	0.0024	0	ILMN_1256343	H19	14955	NA	H19, imprinted maternally expressed transcript
100.4221	1.7744	0.0048	0	ILMN_1252953	Cbln1	12404	869	cerebellin 1 precursor protein
62.1078	1.7686	7.00E-04	0	ILMN_2617162	Mlp	17357	65108	MARCKS-like 1
83.6683	1.7607	0.0025	0	ILMN_2955919	Mcam	84004	4162	melanoma cell adhesion molecule
70.6284	1.7566	0.001	0	ILMN_1259536	Mog	17441	4340	myelin oligodendrocyte glycoprotein
68.3987	1.753	0.001	0	ILMN_2754447	Mkrn3	22652	7681	makorin, ring finger protein, 3
68.3151	1.7464	0.001	0	ILMN_2597606	Gjc2	118454	57165	gap junction protein, gamma 2
95.7042	1.7345	0.0044	0	ILMN_2544056	Hbb-b1	100503605	3043	hemoglobin, beta adult s chain
76.7826	1.7239	0.0024	0	ILMN_1242456	Kank1	107351	23189	KN motif and ankyrin repeat domains 1
82.1412	1.7197	0.0026	0	ILMN_1237021	Mag	17136	4099	myelin-associated glycoprotein
107.5658	1.7077	0.0049	0	ILMN_2675874	Alas2	11656	212	aminolevulinic acid synthase 2, erythroid
105.2858	1.6961	0.0049	0	ILMN_3161282	Dpysl5	65254	56896	dihydropyrimidinase-like 5
104.9667	1.6801	0.005	0	ILMN_1216452	Hbb-b1	NA	NA	NA
101.7441	1.677	0.0048	0	ILMN_2735184	Col18a1	12822	80781	collagen, type XVIII, alpha 1
165.7567	1.6719	0.0137	1.00E-04	ILMN_1241293	Cldn5	12741	7122	claudin 5
104.234	1.67	0.0051	0	ILMN_2991389	Ly6g6e	70274	NA	lymphocyte antigen 6 complex, locus G6E
109.9056	1.6629	0.006	0	ILMN_3105563	Dmkn	73712	93099	dermokine
100.5225	1.6611	0.0046	0	ILMN_1259039	Sox8	NA	NA	NA
119.8152	1.6562	0.0082	0	ILMN_1236718	Hbb-b1	NA	NA	NA
107.4491	1.6543	0.005	0	ILMN_1234698	Tspan2	70747	10100	tetraspanin 2
114.2191	1.651	0.0071	0	ILMN_2457585	Trp53inp2	68728	58476	transformation related protein 53 inducible nuclear protein 2
127.672	1.6497	0.0091	0	ILMN_2977558	Dapk2	13143	23604	death-associated protein kinase 2
115.4908	1.6484	0.0078	0	ILMN_2777359	Serpinh1	12406	871	serine (or cysteine) peptidase inhibitor, clade H, member 1
133.2106	1.6468	0.009	0	ILMN_2757125	Prc1	233406	9055	protein regulator of cytokinesis 1
168.1391	1.645	0.0138	1.00E-04	ILMN_2440194	5330423I11Rik	NA	NA	NA
133.3424	1.6326	0.0088	0	ILMN_2903945	Gadd45g	23882	10912	growth arrest and DNA-damage-inducible 45 gamma
237.4537	1.6307	0.0286	2.00E-04	ILMN_3159435	Mid1	17318	NA	midline 1
121.1858	1.6264	0.0083	0	ILMN_2598103	Emp2	13731	2013	epithelial membrane protein 2
129.3051	1.6258	0.0091	0	ILMN_1215632	Marcksl1	17357	65108	MARCKS-like 1
132.4496	1.6257	0.0091	0	ILMN_3144289	Traf3	22031	7187	TNF receptor-associated factor 3
139.3631	1.6219	0.0092	0	ILMN_2675000	4930511J11Rik	74720	283953	claudin 26

125.9	1.6217	0.0091	0	ILMN_2439638	Traf3	22031	7187	TNF receptor-associated factor 3
264.9656	1.6146	0.0379	2.00E-04	ILMN_2623983	Egr2	13654	1959	early growth response 2
167.9258	1.6117	0.0141	1.00E-04	ILMN_2506428	Ky	16716	339855	kyphoscoliosis peptidase
149.169	1.6067	0.0109	0	ILMN_2545963	Hbb-b1	NA	NA	NA
147.5637	1.6053	0.0108	0	ILMN_2769490	5430435G22Rik	226421	338382	RIKEN cDNA 5430435G22 gene
216.6505	1.6037	0.0234	1.00E-04	ILMN_2443330	Ttr	22139	7276	transthyretin
147.9521	1.6023	0.0111	0	ILMN_2467151	Cyp11a1	NA	NA	NA
177.2045	1.6005	0.0155	1.00E-04	ILMN_1245549	6330404C01Rik	80982	57214	cell migration inducing protein, hyaluronan binding
156.4386	1.5987	0.0116	0	ILMN_1235571	Cyr61	16007	3491	cysteine rich protein 61
151.0446	1.5966	0.0108	0	ILMN_2784078	Mmp15	17388	4324	matrix metallopeptidase 15
128.5692	1.592	0.0091	0	ILMN_1234099	Fermt1	241639	55612	fermitin family homolog 1 (Drosophila)
153.0722	1.591	0.0109	0	ILMN_2701891	Marcksl1	17357	65108	MARCKS-like 1
169.069	1.5888	0.0138	1.00E-04	ILMN_1255462	Hbb-b1	NA	NA	NA
238.1918	1.5774	0.0283	2.00E-04	ILMN_2750515	Fos	14281	2353	FBJ osteosarcoma oncogene
179.4286	1.5767	0.0157	1.00E-04	ILMN_1258028	Gal3st1	53897	9514	galactose-3-O-sulfotransferase 1
168.0194	1.5754	0.0139	1.00E-04	ILMN_2621544	2700060E02Rik	18074	22795	nidogen 2
179.1935	1.5706	0.0159	1.00E-04	ILMN_2711163	Ctsk	13038	1513	cathepsin K
203.9522	1.5702	0.021	1.00E-04	ILMN_2965660	Apcdd1	494504	147495	adenomatosis polyposis coli down-regulated 1
186.0794	1.5661	0.0162	1.00E-04	ILMN_2778722	Ppapdc1a	381925	196051	phosphatidic acid phosphatase type 2 domain containing 1A
183.6942	1.5565	0.0158	1.00E-04	ILMN_1246139	Cldn11	18417	5010	claudin 11
183.6736	1.5551	0.0161	1.00E-04	ILMN_2838308	Fmo1	14261	2326	flavin containing monooxygenase 1
209.5265	1.5551	0.0219	1.00E-04	ILMN_2769777	Msc	17681	9242	musculin
256.1212	1.5496	0.0346	2.00E-04	ILMN_2703138	Tmem125	230678	128218	transmembrane protein 125
204.0502	1.5465	0.0207	1.00E-04	ILMN_2623184	Nkiras2	71966	28511	NFKB inhibitor interacting Ras-like protein 2
202.9992	1.5454	0.0207	1.00E-04	ILMN_2650447	Col23a1	237759	91522	collagen, type XXIII, alpha 1
215.8733	1.545	0.0231	1.00E-04	ILMN_1239117	Hbb-b1	NA	NA	NA
221.9056	1.5432	0.0251	1.00E-04	ILMN_2638473	1190003M12Rik	68888	NA	gastrokine 3
202.5197	1.5425	0.0208	1.00E-04	ILMN_2753342	Hapln1	12950	1404	hyaluronan and proteoglycan link protein 1
210.5965	1.5409	0.022	1.00E-04	ILMN_2759371	Fgfbp1	14181	9982	fibroblast growth factor binding protein 1
235.9454	1.5331	0.0284	2.00E-04	ILMN_3097381	Mobp	17433	4336	myelin-associated oligodendrocytic basic protein
217.9308	1.5305	0.0236	1.00E-04	ILMN_2909782	Rras2	66922	22800	related RAS viral (r-ras) oncogene homolog 2
229.1399	1.5299	0.0263	1.00E-04	ILMN_2472451	Traf4	22032	9618	TNF receptor associated factor 4

271.8732	1.5286	0.0398	2.00E-04	ILMN_3162060	EG574403	574403	100131897	family with sequence similarity 196, member B
233.6047	1.5221	0.0277	2.00E-04	ILMN_2747923	Slc40a1	53945	30061	solute carrier family 40 (iron-regulated transporter), member 1
227.3295	1.5175	0.0263	1.00E-04	ILMN_2517041	Uhrf1	18140	29128	ubiquitin-like, containing PHD and RING finger domains, 1
280.3468	1.5086	0.0429	3.00E-04	ILMN_1241168	Dok4	114255	55715	docking protein 4
254.0057	1.5079	0.0341	2.00E-04	ILMN_2625854	2310016C16Rik	69590	493869	glutathione peroxidase 8 (putative)
256.2349	1.5077	0.0342	2.00E-04	ILMN_1229726	Fibcd1	98970	84929	fibrinogen C domain containing 1
304.0763	1.5074	0.0497	3.00E-04	ILMN_2522884	9930105H17Rik	NA	NA	NA
270.2753	1.5045	0.0393	2.00E-04	ILMN_2815506	Gamt	14431	2593	guanidinoacetate methyltransferase
262.3132	1.5016	0.0369	2.00E-04	ILMN_2778111	Etv4	18612	2118	ets variant 4
288.425	1.4979	0.0449	3.00E-04	ILMN_2604224	Sema5a	20356	9037	sema domain, seven thrombospondin repeats (type 1 and type 1-like), transmembrane domain (TM) and short cytoplasmic domain, (semaphorin) 5A
268.7263	1.4966	0.039	2.00E-04	ILMN_2688236	Atp2a3	53313	489	ATPase, Ca++ transporting, ubiquitous
284.2455	1.4958	0.044	3.00E-04	ILMN_1236788	Igfbp2	16008	3485	insulin-like growth factor binding protein 2
287.3425	1.492	0.0451	3.00E-04	ILMN_2737479	Slc12a9	83704	56996	solute carrier family 12 (potassium/chloride transporters), member 9
274.5651	1.4905	0.041	3.00E-04	ILMN_1257097	Cnp	12799	1267	2',3'-cyclic nucleotide 3' phosphodiesterase
288.7593	1.4897	0.0446	3.00E-04	ILMN_1219025	9030409G11Rik	71529	23254	kazrin, periplakin interacting protein
297.6994	1.4891	0.0481	3.00E-04	ILMN_1251524	Them4	75778	117145	thioesterase superfamily member 4
303.8564	1.4877	0.0501	3.00E-04	ILMN_1226329	Cd93	17064	22918	CD93 antigen
305.5889	1.4821	0.0492	3.00E-04	ILMN_3126277	Palmd	114301	54873	palmdelphin
299.226	1.4801	0.0486	3.00E-04	ILMN_2655204	Apc	11789	324	adenomatosis polyposis coli
303.6034	1.4788	0.0505	3.00E-04	ILMN_2726030	AB023957	NA	NA	NA
304.1851	1.476	0.0493	3.00E-04	ILMN_2772155	LOC100045780	11492	8728	a disintegrin and metallopeptidase domain 19 (meltrin beta)
326.2746	-1.5473	0.0492	4.00E-04	ILMN_2939681	Lyzs	17110	4069	lysozyme 1
324.3234	-1.5513	0.0485	4.00E-04	ILMN_2718266	Fkbp5	14229	2289	FK506 binding protein 5
300.7726	-1.5755	0.0398	3.00E-04	ILMN_2775885	Calm2	12314	NA	calmodulin 2
278.2959	-1.5868	0.0343	2.00E-04	ILMN_1224363	Slc12a5	57138	57468	solute carrier family 12, member 5
281.5906	-1.6113	0.0347	3.00E-04	ILMN_1251998	Gm765	330390	NA	predicted gene 765
226.9486	-1.6145	0.0249	1.00E-04	ILMN_2488510	Ppm1k	243382	152926	protein phosphatase 1K (PP2C domain containing)
308.258	-1.6168	0.0431	3.00E-04	ILMN_1248368	Mat2a	232087	4144	methionine adenosyltransferase II, alpha
275.8602	-1.6184	0.0343	2.00E-04	ILMN_2669088	4930461P20Rik	78244	134218	DnaJ (Hsp40) homolog, subfamily C, member 21

253.8942	-1.62	0.0298	2.00E-04	ILMN_2435835	Evpl	14027	2125	envoplakin
197.6328	-1.6297	0.0211	1.00E-04	ILMN_2602387	Nr1d2	353187	9975	nuclear receptor subfamily 1, group D, member 2
311.5841	-1.6329	0.0428	3.00E-04	ILMN_2734000	Elavl4	15572	1996	ELAV (embryonic lethal, abnormal vision, Drosophila)-like 4 (Hu antigen D)
311.1495	-1.6404	0.043	3.00E-04	ILMN_2859032	Gfod1	328232	54438	glucose-fructose oxidoreductase domain containing 1
253.0893	-1.6455	0.0299	2.00E-04	ILMN_2445958	Tssc8	63830	NA	KCNQ1 overlapping transcript 1
258.1943	-1.6504	0.0299	2.00E-04	ILMN_2419660	mtDNA_ND4L	NA	NA	NA
215.9199	-1.6523	0.0237	1.00E-04	ILMN_1221817	Cd74	16149	972	CD74 antigen (invariant polypeptide of major histocompatibility complex, class II antigen-associated)
308.2304	-1.6595	0.0434	3.00E-04	ILMN_2545149	Nos1ap	70729	NA	nitric oxide synthase 1 (neuronal) adaptor protein
256.5251	-1.6631	0.0294	2.00E-04	ILMN_1219573	C130072A16Rik	105727	81539	solute carrier family 38, member 1
292.3656	-1.6664	0.0367	3.00E-04	ILMN_2475376	BC044804	NA	NA	NA
229.2861	-1.6683	0.0251	1.00E-04	ILMN_1253544	2900060B14Rik	68204	NA	RIKEN cDNA 2900060B14 gene
318.4001	-1.6694	0.0454	4.00E-04	ILMN_1246494	LOC381445	26422	26960	neurobeachin
282.6027	-1.6717	0.0345	3.00E-04	ILMN_2666980	Bdnf	12064	627	brain derived neurotrophic factor
219.961	-1.6722	0.0236	1.00E-04	ILMN_1231445	Inmt	21743	11185	indolethylamine N-methyltransferase
240.372	-1.6762	0.0269	2.00E-04	ILMN_1240202	Fnip1	216742	96459	folliculin interacting protein 1
269.2034	-1.6764	0.033	2.00E-04	ILMN_2987863	Per2	18627	8864	period circadian clock 2
201.3209	-1.677	0.0212	1.00E-04	ILMN_3157692	Ankrd35	213121	148741	ankyrin repeat domain 35
310.3109	-1.679	0.0432	3.00E-04	ILMN_1218471	3-Sep	24050	55964	septin 3
229.1441	-1.6798	0.0254	1.00E-04	ILMN_1229216	Zbtb16	235320	7704	zinc finger and BTB domain containing 16
264.7303	-1.6841	0.0316	2.00E-04	ILMN_1253985	A330021D07Rik	NA	NA	NA
171.7223	-1.6861	0.0163	1.00E-04	ILMN_1235966	Alox12b	11686	242	arachidonate 12-lipoxygenase, 12R type
253.9144	-1.6861	0.0295	2.00E-04	ILMN_1245687	Ash1l	192195	55870	ash1 (absent, small, or homeotic)-like (Drosophila)
294.7856	-1.6875	0.0375	3.00E-04	ILMN_2674890	Tbl1x	21372	6907	transducin (beta)-like 1 X-linked
267.8862	-1.6889	0.0328	2.00E-04	ILMN_2828916	Frmd6	319710	122786	FERM domain containing 6
254.4102	-1.6932	0.0293	2.00E-04	ILMN_1228077	6330437B22Rik	78283	256714	MAP7 domain containing 2
282.4957	-1.6935	0.0347	3.00E-04	ILMN_2589525	Cpeb3	208922	22849	cytoplasmic polyadenylation element binding protein 3
277.0563	-1.6955	0.0345	2.00E-04	ILMN_2466121	Twistnb	28071	221830	TWIST neighbor
250.5161	-1.6978	0.029	2.00E-04	ILMN_2514631	scl0002315.1_12	217869	1983	eukaryotic translation initiation factor 5
186.3783	-1.7007	0.0195	1.00E-04	ILMN_2493030	2310043N10Rik	66961	NA	nuclear paraspeckle assembly transcript 1 (non-protein coding)

263.9285	-1.7033	0.0315	2.00E-04	ILMN_2677270	Peg3	18616	5178	paternally expressed 3
239.6678	-1.7039	0.0271	2.00E-04	ILMN_1214405	Cnksr2	245684	22866	connector enhancer of kinase suppressor of Ras 2
253.7716	-1.7042	0.03	2.00E-04	ILMN_2763404	Nrxn3	18191	NA	neurexin III
182.2435	-1.7079	0.0186	1.00E-04	ILMN_1246861	Ctss	13040	1520	cathepsin S
278.7674	-1.7082	0.0341	2.00E-04	ILMN_1239608	Arid4a	238247	5926	AT rich interactive domain 4A (RBP1-like)
242.1379	-1.7088	0.0269	2.00E-04	ILMN_2745614	Fam134b	66270	54463	family with sequence similarity 134, member B
273.3035	-1.7094	0.0336	2.00E-04	ILMN_2762701	Scn1a	20265	6323	sodium channel, voltage-gated, type I, alpha
235.4555	-1.7097	0.0263	2.00E-04	ILMN_1243910	Zfp292	30046	23036	zinc finger protein 292
182.6041	-1.71	0.0184	1.00E-04	ILMN_2690603	Spp1	20750	6696	secreted phosphoprotein 1
262.6651	-1.7167	0.0313	2.00E-04	ILMN_2733314	Rgs7bp	52882	401190	regulator of G-protein signalling 7 binding protein
218.5161	-1.7173	0.0237	1.00E-04	ILMN_2593368	Mat2a	232087	4144	methionine adenosyltransferase II, alpha
248.3251	-1.7218	0.0284	2.00E-04	ILMN_2525034	Cc1	12421	9821	RB1-inducible coiled-coil 1
244.6249	-1.7232	0.0273	2.00E-04	ILMN_2713008	C030011O14Rik	215708	374986	family with sequence similarity 73, member A
244.4499	-1.7244	0.0276	2.00E-04	ILMN_1228020	1500010G04Rik	NA	NA	NA
214.8649	-1.7247	0.0242	1.00E-04	ILMN_2664706	Chic1	12212	53344	cysteine-rich hydrophobic domain 1
224.3588	-1.7256	0.0252	1.00E-04	ILMN_1251488	A430041B07Rik	328108	23116	family with sequence similarity 179, member B
167.7266	-1.7283	0.0158	1.00E-04	ILMN_2651054	LOC100047173	269589	84958	synaptotagmin-like 1
233.1724	-1.7313	0.0262	2.00E-04	ILMN_2713004	C030011O14Rik	215708	374986	family with sequence similarity 73, member A
224.4289	-1.7346	0.0249	1.00E-04	ILMN_1233554	Pbrm1	66923	55193	polybromo 1
215.0498	-1.7355	0.0239	1.00E-04	ILMN_2669461	Bbx	70508	56987	bobby sox homolog (Drosophila)
220.6021	-1.7382	0.0238	1.00E-04	ILMN_1218712	Jph4	NA	NA	NA
229.662	-1.7394	0.0248	1.00E-04	ILMN_1231596	Mtap7	NA	NA	NA
217.0292	-1.7397	0.0237	1.00E-04	ILMN_2492395	2900064A13Rik	NA	NA	NA
194.6882	-1.7416	0.0213	1.00E-04	ILMN_1218051	Iqgap2	544963	10788	IQ motif containing GTPase activating protein 2
224.9623	-1.7422	0.0249	1.00E-04	ILMN_1220626	2010007K12Rik	NA	NA	NA
193.5535	-1.7437	0.0213	1.00E-04	ILMN_2689307	Spnb2	20742	6711	spectrin beta, non-erythrocytic 1
211.5491	-1.7446	0.0235	1.00E-04	ILMN_2594593	Mpp5	56217	64398	membrane protein, palmitoylated 5 (MAGUK p55 subfamily member 5)
196.6783	-1.7461	0.0214	1.00E-04	ILMN_2541675	LOC382128	319675	85459	RIKEN cDNA 5830418K08 gene
225.9716	-1.7473	0.0251	1.00E-04	ILMN_1230605	Gm336	212285	116984	ArfGAP with RhoGAP domain, ankyrin repeat and PH domain 2
172.8921	-1.7587	0.0162	1.00E-04	ILMN_2803674	S100a9	20202	6280	S100 calcium binding protein A9 (calgranulin B)
192.6629	-1.759	0.0213	1.00E-04	ILMN_3072536	Eif5	217869	1983	eukaryotic translation initiation factor 5
138.7531	-1.7606	0.0112	0	ILMN_1255416	Ly6a	110454	NA	lymphocyte antigen 6 complex, locus A

206.7346	-1.7624	0.0217	1.00E-04	ILMN_2596077	2810474O19Rik	67246	55196	RIKEN cDNA 2810474O19 gene
190.8274	-1.7627	0.0211	1.00E-04	ILMN_1237335	A730028C12Rik	NA	NA	NA
197.1239	-1.7662	0.0214	1.00E-04	ILMN_2593230	Mllt4	17356	4301	myeloid/lymphoid or mixed-lineage leukemia (trithorax homolog, Drosophila); translocated to, 4
200.8213	-1.769	0.0212	1.00E-04	ILMN_2595282	2600005C20Rik	72462	23076	ribosomal RNA processing 1 homolog B (S. cerevisiae)
200.7106	-1.7702	0.0215	1.00E-04	ILMN_2481389	Zfp326	54367	284695	zinc finger protein 326
164.0235	-1.774	0.0155	1.00E-04	ILMN_1220828	2900075B16Rik	78506	286097	mitochondrial calcium uptake family, member 3
155.2155	-1.7756	0.0142	0	ILMN_2571934	D030034I04Rik	105727	81539	solute carrier family 38, member 1
176.004	-1.7781	0.0166	1.00E-04	ILMN_1229727	Gpr123	52389	84435	G protein-coupled receptor 123
175.0744	-1.7835	0.0164	1.00E-04	ILMN_1237059	Kcna1	16485	3736	potassium voltage-gated channel, shaker-related subfamily, member 1
152.5807	-1.7867	0.014	0	ILMN_2512204	mt-Nd4l	NA	NA	NA
191.3641	-1.7915	0.021	1.00E-04	ILMN_1236941	Csnk2a1-rs3	12995	1457	casein kinase 2, alpha 1 polypeptide
117.9399	-1.796	0.0095	0	ILMN_2629112	Asah3l	230379	340485	alkaline ceramidase 2
154.7781	-1.7976	0.0144	0	ILMN_2423249	2010321I05Rik	233833	27327	trinucleotide repeat containing 6a
169.376	-1.7979	0.0157	1.00E-04	ILMN_1260446	Ttc3	22129	7267	tetratricopeptide repeat domain 3
159.9385	-1.8005	0.0148	0	ILMN_3151492	Ankrd12	106585	23253	ankyrin repeat domain 12
159.7083	-1.8008	0.0149	0	ILMN_2747381	Ddx24	27225	57062	DEAD (Asp-Glu-Ala-Asp) box polypeptide 24
117.7708	-1.806	0.0094	0	ILMN_2746797	Hsf4	26386	3299	heat shock transcription factor 4
154.9416	-1.8113	0.0141	0	ILMN_1227149	Meg3	17263	NA	maternally expressed 3
154.4618	-1.8188	0.0141	0	ILMN_2544603	2610015J01Rik	67039	NA	RNA binding motif protein 25
149.6626	-1.8218	0.0137	0	ILMN_1234357	A230057E24Rik	NA	NA	NA
160.7228	-1.8235	0.0145	0	ILMN_2737867	Mtap1b	17755	4131	microtubule-associated protein 1B
146.4398	-1.8285	0.0132	0	ILMN_2657911	Cnot4	53621	4850	CCR4-NOT transcription complex, subunit 4
137.4716	-1.8312	0.0115	0	ILMN_2654932	Pdap1	231887	11333	PDGFA associated protein 1
149.0718	-1.8342	0.0133	0	ILMN_2542231	LOC382157	228005	9360	peptidyl-prolyl isomerase G (cyclophilin G)
136.8161	-1.8372	0.0118	0	ILMN_1256701	2900016B01Rik	74901	9920	kelch repeat and BTB (POZ) domain containing 11
140.2596	-1.8406	0.0112	0	ILMN_1217776	Mll5	69188	55904	lysine (K)-specific methyltransferase 2E
123.3913	-1.8632	0.0097	0	ILMN_2466797	scl0001284.1_18	NA	NA	NA
120.66	-1.8657	0.0092	0	ILMN_2495555	Mapk8ip2	NA	NA	NA
110.3349	-1.8716	0.008	0	ILMN_2720479	Lpgat1	226856	9926	lysophosphatidylglycerol acyltransferase 1
107.1799	-1.8815	0.0084	0	ILMN_3031781	Arid5b	71371	84159	AT rich interactive domain 5B (MRF1-like)
108.2637	-1.8822	0.0082	0	ILMN_2968123	Slc7a14	241919	57709	solute carrier family 7 (cationic amino acid

								transporter, y+ system), member 14
102.8964	-1.8896	0.0082	0	ILMN_2524100	Zswim6	67263	57688	zinc finger SWIM-type containing 6
106.148	-1.8943	0.008	0	ILMN_1243996	Ash1l	192195	55870	ash1 (absent, small, or homeotic)-like (Drosophila)
108.9677	-1.8986	0.0082	0	ILMN_1226085	Syt1	NA	NA	NA
99.6837	-1.8993	0.0081	0	ILMN_2844963	Nos1ap	70729	NA	nitric oxide synthase 1 (neuronal) adaptor protein
80.4955	-1.9004	0.0043	0	ILMN_3107059	Espn	56226	83715	espin
150.8775	-1.9026	0.0136	0	ILMN_1245389	LOC236604	236604	NA	phosphatidylserine decarboxylase, pseudogene 1
99.2247	-1.9029	0.0085	0	ILMN_2715848	Slitrk4	245446	139065	SLIT and NTRK-like family, member 4
104.8752	-1.9033	0.0083	0	ILMN_2771709	Ppargc1b	170826	133522	peroxisome proliferative activated receptor, gamma, coactivator 1 beta
93.2724	-1.922	0.0076	0	ILMN_3028837	Pcdh9	211712	5101	protocadherin 9
70.0507	-1.9234	0.0043	0	ILMN_2752883	Hsp90aa1	15519	3320	heat shock protein 90, alpha (cytosolic), class A member 1
68.4948	-1.9249	0.0045	0	ILMN_2702303	Ch25h	12642	9023	cholesterol 25-hydroxylase
78.6377	-1.9335	0.0045	0	ILMN_3144164	Irs2	384783	8660	insulin receptor substrate 2
83.4984	-1.9539	0.005	0	ILMN_1255854	Mtap9	213582	79884	microtubule-associated protein 9
62.4352	-1.9916	0.0039	0	ILMN_2639442	Rock2	19878	9475	Rho-associated coiled-coil containing protein kinase 2
65.2953	-2.006	0.0047	0	ILMN_2703913	Mtf2	17765	22823	metal response element binding transcription factor 2
57.2834	-2.0145	0.0018	0	ILMN_1236844	A830094I09Rik	NA	NA	NA
55.3183	-2.0239	0.0021	0	ILMN_1236820	9430047F21Rik	NA	NA	NA
55.866	-2.0392	0.0019	0	ILMN_2432200	Epb4.1	NA	NA	NA
49.8425	-2.0396	0.0023	0	ILMN_2642426	Agmat	75986	79814	agmatine ureohydrolase (agmatinase)
45.5522	-2.0743	0.0017	0	ILMN_1237548	5830407P18Rik	NA	NA	NA
44.5367	-2.0756	0.0018	0	ILMN_1259747	Il33	77125	90865	interleukin 33
40.11	-2.0942	0.001	0	ILMN_3124885	Pdpk1	18607	5170	3-phosphoinositide dependent protein kinase 1
35.7678	-2.1106	0	0	ILMN_2601176	Meg3	17263	NA	maternally expressed 3
38.3554	-2.1249	0.0011	0	ILMN_1225423	Mslnl	328783	NA	mesothelin-like
55.718	-2.1295	0.002	0	ILMN_2668333	Prg4	96875	NA	proteoglycan 4 (megakaryocyte stimulating factor, articular superficial zone protein)
27.1219	-2.1716	0	0	ILMN_1216085	B230387C07Rik	106585	23253	ankyrin repeat domain 12
25.1926	-2.2119	0	0	ILMN_1238436	Cplx2	12890	10814	complexin 2
107.5742	-2.2202	0.0081	0	ILMN_2965669	Xlr4a	NA	NA	NA
28.7047	-2.2624	0	0	ILMN_2661820	Agxt2l1	71760	64850	ethanolamine phosphate phospholyase

23.2317	-2.4004	0	0	ILMN_2652500	Lrg1	76905	116844	leucine-rich alpha-2-glycoprotein 1
11.5889	-2.5107	0	0	ILMN_1229990	Agxt2l1	71760	64850	ethanolamine phosphate phospholyase
14.3442	-2.7824	0	0	ILMN_2710905	S100a8	20201	6279	S100 calcium binding protein A8 (calgranulin A)
3.6486	-3.7411	0	0	ILMN_2712075	Lcn2	16819	3934	lipocalin 2

Table 2. Molecular matching between 436 disease signatures and the juvenile plasticity signature indicates diverse diseases may disrupt plasticity.

Rank	Normalized molecular match score	Emp_pval	FDR	Source_dat	Species	Disease	Tissue
1	9.64	4.53E-08	1.22E-05	GSE7958	Mus musculus	Huntington's Disease	CNS - Brain - Striatum (MMHCC)
2	8.35	7.74E-08	1.22E-05	GSE1623	Mus musculus	Type 1 diabetes mellitus	Pancreas
3	8.32	8.58E-07	3.40E-05	GSE9857	Mus musculus	Huntington's Disease	CNS - Brain - Striatum (MMHCC)
4	7.96	1.38E-07	1.22E-05	GSE4648	Mus musculus	Acute myocardial infarction	Myocardial tissue
5	7.59	1.40E-07	1.22E-05	GSE4290	Homo sapiens	Glioblastoma	CNS - Brain (MMHCC)
6	7.52	3.36E-07	2.44E-05	GSE1481	Homo sapiens	Anterior Horn Cell Disease	CNS - Spinal Cord (MMHCC)
7	6.81	9.04E-08	1.22E-05	GSE2240	Homo sapiens	Atrial Fibrillation	Myocardial tissue
8	6.73	1.47E-06	4.94E-05	GSE5500	Mus musculus	Cardiac Hypertrophy	Myocardial tissue
9	6.47	8.10E-07	3.40E-05	GSE5389	Homo sapiens	Bipolar Disorder	frontal cortex
10	6.33	8.15E-07	3.40E-05	GSE5078	Mus musculus	Senescence	Hippocampus
11	6.25	1.75E-06	5.46E-05	GSE4764	Mus musculus	Yersinia enterocolitica food poisoning	Peyer's patch
12	5.75	7.82E-07	3.40E-05	GSE4290	Homo sapiens	Astrocytoma	CNS - Brain (MMHCC)
13	5.7	1.73E-05	3.59E-04	GSE1621	Mus musculus	Cardiac Hypertrophy	Myocardial tissue
14	5.67	6.55E-05	7.88E-04	GSE3253	Mus musculus	Bacterial Infection	CNS - Brain (MMHCC)
15	5.61	1.16E-06	4.22E-05	GSE10599	Mus musculus	Spinal Muscular Atrophy	Kidney
16	5.55	2.49E-06	7.25E-05	GSE3744	Homo sapiens	Breast Cancer	Mammary Gland Tissue
17	5.43	1.32E-05	3.04E-04	GSE6731	Homo sapiens	Crohn's disease	Intestine - Large Intestine - Colon (MMHCC)
18	5.38	2.24E-05	4.24E-04	GSE6731	Homo sapiens	Ulcerative Colitis	Intestine - Large Intestine - Colon (MMHCC)
19	5.35	1.29E-05	3.04E-04	GSE11343	Mus musculus	Diabetic Neuropathy	Sciatic Nerve
20	5.35	7.33E-07	3.40E-05	GSE4316	Homo sapiens	Primary open angle glaucoma	Trabecular Meshwork
21	5.28	2.67E-05	4.65E-04	GSE5406	Homo sapiens	Cardiomyopathy	Myocardial tissue
22	5.02	3.36E-05	5.29E-04	GSE464	Rattus norvegicus	Spinal Cord Injury	CNS - Spinal Cord (MMHCC)
23	4.98	1.87E-05	3.71E-04	EXPE-MEXP-567	Homo sapiens	Glioblastoma	Brain
24	4.94	1.17E-04	1.13E-03	GSE1025	Mus musculus	Duchenne muscular dystrophy (DMD)	Muscle - Striated (Skeletal) (MMHCC)
25	4.9	5.26E-05	6.95E-04	GSE1843	Rattus norvegicus	Hepatic Cirrhosis	Hepatic Tissue
26	4.86	1.54E-05	3.37E-04	GSE1572	Homo sapiens	Senescence	frontal cortex
27	4.81	6.87E-05	7.88E-04	GSE1472	Mus musculus	Duchenne muscular dystrophy (DMD)	Muscle - Striated (Skeletal) (MMHCC)
28	4.81	9.47E-06	2.43E-04	GSE2510	Homo sapiens	Obesity	Adipocyte

29	4.8	3.91E-05	5.49E-04	GSE3383	Mus musculus	Cardiac Hypertrophy	Myocardial tissue
30	4.78	1.06E-04	1.05E-03	GSE1629	Homo sapiens	Dental cavity, complex	Dental Pulp
31	4.72	6.79E-05	7.88E-04	GSE2629	Mus musculus	Muscular Dystrophy	Muscle - Striated (Skeletal) (MMHCC)
32	4.67	3.90E-05	5.49E-04	GSE4290	Homo sapiens	Oligodendroglioma	CNS - Brain (MMHCC)
33	4.63	1.71E-04	1.49E-03	GSE10760	Homo sapiens	Muscular Dystrophy	Musculus vastus lateralis
34	4.62	9.53E-05	1.01E-03	GSE1988	Mus musculus	Cardiac Failure	Myocardial tissue
35	4.61	4.84E-05	6.59E-04	GSE3467	Homo sapiens	Papillary Carcinoma of the Thyroid	Thyroid Gland (MMHCC)
36	4.57	3.84E-05	5.49E-04	GSE3621	Mus musculus	Huntington's Disease	Brain
37	4.56	3.35E-05	5.29E-04	GSE4107	Homo sapiens	Cancer of Colon	Intestine - Large Intestine - Colon (MMHCC)
38	4.54	1.20E-04	1.14E-03	GSE842	Mus musculus	MS (Multiple Sclerosis)	CNS - Spinal Cord (MMHCC)
39	4.53	8.18E-05	9.14E-04	GSE14905	Homo sapiens	Psoriasis vulgaris	Skin tissue
40	4.51	3.40E-05	5.29E-04	GSE7305	Homo sapiens	Endometriosis	Endometrium
41	4.48	8.91E-06	2.43E-04	GSE16524	Homo sapiens	Setleis syndrome	Skin fibroblast
42	4.46	6.85E-05	7.88E-04	GSE4183	Homo sapiens	Carcinoma in situ of large intestine	Colon
43	4.43	2.37E-05	4.30E-04	GSE12654	Homo sapiens	Schizophrenia	Cerebral cortex
44	4.3	1.62E-04	1.44E-03	GSE2866	Mus musculus	Gamma-hydroxybutyric acidaemia	CNS - Brain - Cerebellum (MMHCC)
45	4.22	9.23E-05	1.01E-03	GSE1859	Mus musculus	FDIU - Fetal death in utero	Hepatic Tissue
46	4.19	5.52E-05	7.08E-04	GSE4587	Homo sapiens	Malignant Melanoma	Epidermis
47	4.16	2.13E-04	1.82E-03	GSE63	Mus musculus	Cerebral Infarction	CNS - Brain (MMHCC)
48	4.16	2.26E-04	1.83E-03	GSE6614	Mus musculus	Generalized seizures	Brain
49	4.08	1.58E-04	1.44E-03	GSE6280	Homo sapiens	Chronic kidney disease	Kidney
50	4.01	3.19E-04	2.44E-03	GSE5390	Homo sapiens	Down Syndrome	Brain
51	4.01	2.66E-04	2.11E-03	GSE2052	Homo sapiens	Idiopathic fibrosing alveolitis	Lung Tissue
52	4	2.23E-04	1.83E-03	GSE1873	Mus musculus	Obstructive sleep apnea	Hepatic Tissue
53	3.97	4.39E-04	3.07E-03	GSE4183	Homo sapiens	IBD - Inflammatory bowel disease	Colon
54	3.96	1.01E-04	1.02E-03	GSE3075	Mus musculus	Spinal Muscular Atrophy, Infantile	CNS - Spinal Cord (MMHCC)
55	3.94	1.42E-04	1.32E-03	GSE3167	Homo sapiens	Urothelial carcinoma in situ	Urothelium
56	3.93	2.20E-04	1.83E-03	GSE8514	Homo sapiens	Adenoma	Adrenal gland
57	3.93	4.01E-04	2.92E-03	GSE6764	Homo sapiens	Carcinoma, Hepatocellular	Liver
58	3.92	4.89E-04	3.18E-03	GSE3585	Homo sapiens	Cardiomyopathy, Dilated	Myocardial tissue
59	3.89	3.39E-04	2.55E-03	GSE1420	Homo sapiens	Barrett Esophagus	Esophageal Tissue
60	3.88	9.89E-05	1.02E-03	GSE1420	Homo sapiens	Adenocarcinoma of esophagus	Esophageal Tissue
61	3.87	4.40E-04	3.07E-03	GSE781	Homo sapiens	Clear cell carcinoma of kidney	Renal Tissue

62	3.87	5.95E-04	3.51E-03	GSE2528	Mus musculus	Breast Cancer	Mammary gland
63	3.84	9.37E-04	4.92E-03	GSE1026	Mus musculus	Duchenne muscular dystrophy (DMD)	Muscle - Striated (Skeletal) - Diaphragm (MMHCC)
64	3.79	5.25E-04	3.35E-03	GSE3678	Homo sapiens	Papillary Carcinoma of the Thyroid	Thyroid Gland (MMHCC)
65	3.74	4.88E-04	3.18E-03	GSE4619	Homo sapiens	MDS - Myelodysplastic syndrome	Bone marrow stem cell
66	3.73	5.92E-04	3.51E-03	GSE3112	Homo sapiens	Polymyositis	Muscle tissue
67	3.72	3.51E-04	2.59E-03	GSE3189	Homo sapiens	Multiple benign melanocytic nevi	Epidermis
68	3.68	5.76E-04	3.49E-03	GSE769	Mus musculus	Cystic Fibrosis	Pancreas
69	3.66	5.76E-04	3.49E-03	GSE10432	Homo sapiens	Acne	Sebocyte
70	3.65	1.30E-03	6.16E-03	GSE3252	Mus musculus	Muscular Dystrophy	Muscle - Striated (Skeletal) - Diaphragm (MMHCC)
71	3.62	4.81E-04	3.18E-03	GSE12649	Homo sapiens	Schizophrenia	Cerebral cortex
72	3.6	7.41E-04	4.17E-03	GSE2501	Mus musculus	Thymic Carcinoma	Thymus
73	3.59	1.20E-03	5.87E-03	GSE3268	Homo sapiens	Squamous cell carcinoma of lung	Lung Tissue
74	3.58	7.82E-04	4.32E-03	GSE857	Mus musculus	Huntington's Disease	CNS - Brain (MMHCC)
75	3.58	2.96E-04	2.30E-03	GSE1009	Homo sapiens	Diabetic Nephropathy	Renal Tissue
76	3.57	1.20E-03	5.87E-03	GSE977	Mus musculus	Alexander Disease	CNS - Brain - Olfactory Bulb (MMHCC)
77	3.55	5.37E-04	3.35E-03	GSE2826	Mus musculus	Bruton's agammaglobulinemia	B Cell Lymphocyte
78	3.54	7.46E-04	4.17E-03	GSE2640	Mus musculus	Pulmonary Fibrosis	Lung Tissue
79	3.53	5.37E-04	3.35E-03	GSE2514	Homo sapiens	Adenocarcinoma of lung	Lung Tissue
80	3.53	8.90E-04	4.73E-03	GSE1551	Homo sapiens	Dermatomyositis	Muscle - Striated (Skeletal) (MMHCC)
81	3.52	4.50E-04	3.07E-03	GSE2507	Mus musculus	Muscular Dystrophy	Muscle - Striated (Skeletal) (MMHCC)
82	3.5	7.15E-04	4.10E-03	GSE3189	Homo sapiens	Malignant Melanoma	Epidermis
83	3.5	1.10E-03	5.58E-03	GSE4764	Mus musculus	Yersinia enterocolitica food poisoning	Lymph node
84	3.45	8.68E-04	4.67E-03	EXPE-MEXP-567	Homo sapiens	Glioblastoma	Brain
85	3.43	4.44E-04	3.07E-03	GSE3408	Homo sapiens	Atypical mycobacterial infection	macrophage
86	3.43	1.10E-03	5.58E-03	GSE6428	Rattus norvegicus	Type 2 diabetes mellitus	Endocrine Pancreas - Islet Cell of Langerhans - Beta Cell (MMHCC)
87	3.42	8.45E-04	4.61E-03	GSE10575	Homo sapiens	Arthropathy	Chondrocyte
88	3.4	6.73E-04	3.91E-03	GSE9375	Mus musculus	Huntington's Disease	CNS - Brain - Striatum (MMHCC)
89	3.39	2.10E-03	9.16E-03	GSE4390	Mus musculus	ALS (Amyotrophic Lateral Sclerosis)	CNS - Spinal Cord (MMHCC)
90	3.38	1.21E-03	5.87E-03	GSE3644	Mus musculus	Acute pancreatitis	Pancreas
91	3.38	1.30E-03	6.16E-03	GSE3112	Homo sapiens	Inclusion Body Myositides	Muscle tissue
92	3.33	1.10E-03	5.58E-03	GSE466	Mus musculus	Duchenne muscular dystrophy (DMD)	Muscle - Striated (Skeletal) (MMHCC)
93	3.29	1.40E-03	6.36E-03	GSE2144	Homo sapiens	GERD - Gastro-esophageal reflux	Esophageal Tissue

						disease	
94	3.27	1.40E-03	6.36E-03	EXPE-MEXP-1296	Mus musculus	Cancer of prostate	Prostate
95	3.24	1.70E-03	7.64E-03	GSE2724	Homo sapiens	Uterine leiomyoma	Uterus
96	3.21	3.30E-03	1.30E-02	GSE2825	Rattus norvegicus	Idiosyncratic drug effect	Hepatic Tissue
97	3.19	2.60E-03	1.08E-02	GSE1007	Homo sapiens	Duchenne muscular dystrophy (DMD)	Muscle - Striated (Skeletal) (MMHCC)
98	3.19	1.20E-03	5.87E-03	GSE1781	Rattus norvegicus	Sepsis	Hepatic Tissue
99	3.18	2.40E-03	1.03E-02	GSE2899	Mus musculus	Type 2 diabetes mellitus	Adipose tissue
100	3.18	1.90E-03	8.37E-03	GSE2557	Mus musculus	Kidney disorder associated with type 2 diabetes mellitus	Mesangial cell
101	3.18	1.40E-03	6.36E-03	GSE3524	Homo sapiens	Squamous cell carcinoma of mouth	Oropharynx Epithelium
102	3.17	1.40E-03	6.36E-03	GSE13355	Homo sapiens	Psoriasis vulgaris	Skin tissue
103	3.15	2.20E-03	9.50E-03	GSE2866	Mus musculus	Gamma-hydroxybutyric acidaemia	Cerebral cortex
104	3.12	2.60E-03	1.08E-02	GSE4911	Mus musculus	Cleidocranial dysostosis	Humerus
105	3.12	1.90E-03	8.37E-03	GSE24807	Homo sapiens	NASH	Liver
106	3.12	3.20E-03	1.28E-02	GSE10631	Homo sapiens	LGLL - Large granular lymphocytic leukemia	Peripheral blood mononuclear cell
107	3.11	2.70E-03	1.11E-02	GSE2052	Homo sapiens	Scleroderma	Lung Tissue
108	3.07	2.90E-03	1.17E-02	GSE4692	Mus musculus	Obesity	Adipose tissue
109	3.05	2.50E-03	1.06E-02	GSE4824	Homo sapiens	Non-small cell lung cancer	Bronchial epithelium
110	3.03	3.80E-03	1.47E-02	GSE1145	Homo sapiens	Ischaemic cardiomyopathy	Myocardial tissue
111	3.01	4.90E-03	1.77E-02	GSE6678	Mus musculus	Infantile neuronal ceroid lipofuscinosis	Brain
112	3	3.30E-03	1.30E-02	GSE3064	Homo sapiens	Dystonia	Brain
113	2.99	4.70E-03	1.72E-02	GSE2527	Mus musculus	Thrombocytopenia	Megakaryocyte
114	2.99	4.30E-03	1.62E-02	GSE2433	Mus musculus	Leukemia, Acute Megakaryocytic	Megakaryocyte
115	2.93	4.60E-03	1.71E-02	GSE1776	Mus musculus	Nutritional deficiency, NEC	Skeletal Myocyte
116	2.93	3.90E-03	1.49E-02	GSE4587	Homo sapiens	In situ melanoma of skin	Epidermis
117	2.92	5.30E-03	1.88E-02	GSE9579	Homo sapiens	Appendicitis	Appendix
118	2.91	5.80E-03	2.01E-02	GSE2411	Mus musculus	Ventilator-associated lung injury	Lung Tissue
119	2.9	2.80E-03	1.14E-02	GSE1037	Homo sapiens	Small cell carcinoma of lung	Lung Tissue
120	2.86	5.20E-03	1.86E-02	GSE2401	Rattus norvegicus	Hypotensive episode	Renal Tissue
121	2.85	4.70E-03	1.72E-02	GSE765	Mus musculus	Cystic Fibrosis	Intestinal Epithelium
122	2.83	3.60E-03	1.40E-02	EXPE-MEXP-882	Homo sapiens	Invasive ductal breast cancer	Mammary Epithelium
123	2.83	6.70E-03	2.28E-02	GSE1869	Homo sapiens	Ischaemic cardiomyopathy	Myocardial tissue

124	2.82	5.60E-03	1.95E-02	GSE4183	Homo sapiens	Adenoma	Colon
125	2.82	5.40E-03	1.90E-02	GSE1004	Homo sapiens	Duchenne muscular dystrophy (DMD)	Muscle - Striated (Skeletal) (MMHCC)
126	2.81	4.30E-03	1.62E-02	GSE9944	Homo sapiens	Glaucoma	Astrocyte
127	2.79	6.20E-03	2.13E-02	EXPE-TABM-176	Homo sapiens	Irritable bowel syndrome variant of childhood with diarrhea	Sigmoid colon
128	2.72	8.40E-03	2.75E-02	GSE2779	Homo sapiens	MDS - Myelodysplastic syndrome	Bone marrow stem cell
129	2.72	7.20E-03	2.43E-02	GSE1947	Mus musculus	Peripheral motor neuropathy	Sciatic Nerve
130	2.71	8.40E-03	2.75E-02	GSE593	Homo sapiens	Uterine leiomyoma	Uterus - Myometrium (MMHCC)
131	2.71	7.50E-03	2.52E-02	GSE2712	Homo sapiens	Clear cell sarcoma of kidney	Renal Tissue
132	2.69	8.50E-03	2.75E-02	GSE1459	Mus musculus	Bacterial Infection	macrophage
133	2.67	8.50E-03	2.75E-02	GSE1811	Mus musculus	Occupational lung disease	Lung Tissue
134	2.67	8.90E-03	2.85E-02	GSE2508	Homo sapiens	Obesity	Adipocyte
135	2.66	8.10E-03	2.70E-02	GSE1462	Homo sapiens	MELAS - Mitochondrial myopathy, encephalopathy, lactic acidosis and stroke-like episodes	Muscle - Striated (Skeletal) (MMHCC)
136	2.65	9.00E-03	2.86E-02	GSE4130	Rattus norvegicus	Dehydration	CNS - Brain - Hypothalamus (MMHCC)
137	2.61	9.10E-03	2.88E-02	GSE1378	Homo sapiens	Breast Cancer	Mammary Gland Tissue
138	2.6	1.14E-02	3.45E-02	GSE1375	Mus musculus	Alzheimer's Disease	Cerebral cortex
139	2.59	9.80E-03	3.03E-02	GSE2719	Homo sapiens	Gastrointestinal stromal tumor	Connective Tissue
140	2.59	9.60E-03	3.01E-02	GSE7036	Homo sapiens	Bipolar Disorder	Lymphocyte
141	2.57	1.00E-02	3.07E-02	GSE1724	Homo sapiens	Scleroderma	Fibroblast
142	2.56	9.70E-03	3.02E-02	GSE3790	Homo sapiens	Huntington's Disease	Caudate Nucleus
143	2.55	1.25E-02	3.68E-02	GSE6764	Homo sapiens	Hepatic Cirrhosis	Liver
144	2.54	1.24E-02	3.68E-02	GSE2457	Rattus norvegicus	Erectile dysfunction associated with type 2 diabetes mellitus	Penis, NOS
145	2.54	1.47E-02	4.14E-02	GSE2457	Rattus norvegicus	Erectile dysfunction	Penis Erectile Tissue
146	2.54	1.05E-02	3.20E-02	GSE3110	Rattus norvegicus	Dehydration	Hypothalamus
147	2.53	1.22E-02	3.64E-02	GSE2712	Homo sapiens	Nephroblastoma	Renal Tissue
148	2.51	1.42E-02	4.05E-02	GSE7999	Rattus norvegicus	Tachycardia	Myocardial tissue
149	2.51	1.29E-02	3.77E-02	GSE609	Homo sapiens	SCID - Severe combined immunodeficiency	Thymic lymphocyte
150	2.49	1.19E-02	3.58E-02	GSE1869	Homo sapiens	Cardiomyopathy	Myocardial tissue
151	2.49	1.36E-02	3.93E-02	GSE7621	Homo sapiens	Parkinson's Disease	Substantia Nigra
152	2.48	1.35E-02	3.92E-02	GSE10971	Homo sapiens	Serous carcinoma	Fallopian tube
153	2.48	1.40E-02	4.02E-02	GSE3418	Mus musculus	Lung transplant rejection	Trachea

154	2.47	1.45E-02	4.11E-02	EXPE-MEXP-476	Homo sapiens	Cancer of prostate	Endothelial cell
155	2.47	1.54E-02	4.28E-02	GSE3184	Mus musculus	Asthma, allergic	Lung Tissue
156	2.46	1.49E-02	4.16E-02	GSE4616	Mus musculus	Type 1 diabetes mellitus	Myocardial tissue
157	2.41	1.68E-02	4.64E-02	GSE4612	Mus musculus	Carcinoma, Hepatocellular	Hepatic Tissue
158	2.4	1.77E-02	4.85E-02	GSE2725	Homo sapiens	Uterine leiomyoma	Uterus
159	2.39	1.81E-02	4.90E-02	GSE3365	Homo sapiens	Ulcerative Colitis	Peripheral blood mononuclear cell
160	2.37	1.80E-02	4.90E-02	GSE1813	Rattus norvegicus	Obesity	Adipose tissue
161	2.36	1.87E-02	5.03E-02	GSE4060	Homo sapiens	Cushing Syndrome	Adrenal gland
162	2.35	2.07E-02	5.50E-02	GSE1145	Homo sapiens	Primary cardiomyopathy	Myocardial tissue
163	2.31	1.88E-02	5.03E-02	GSE6461	Mus musculus	Synovial sarcoma	Synovial Membrane
164	2.3	2.15E-02	5.68E-02	GSE1037	Homo sapiens	Non-small cell lung cancer	Lung Tissue
165	2.27	2.29E-02	6.01E-02	GSE10921	Homo sapiens	Idiopathic fibrosing alveolitis	Fibroblast
166	2.26	2.41E-02	6.28E-02	GSE3248	Mus musculus	Huntington's Disease	CNS - Brain - Cerebellum (MMHCC)
167	2.25	2.42E-02	6.28E-02	GSE4788	Mus musculus	Parkinson's Disease	Substantia Nigra
168	2.24	2.52E-02	6.46E-02	GSE4710	Mus musculus	Heart Injury	Myocardial tissue
169	2.21	2.52E-02	6.46E-02	GSE6364	Homo sapiens	Endometriosis	Endometrium
170	2.2	2.68E-02	6.83E-02	GSE1462	Homo sapiens	CPEO - chronic progressive external ophthalmoplegia	Muscle - Striated (Skeletal) (MMHCC)
171	2.19	3.00E-02	7.56E-02	GSE1724	Homo sapiens	Idiopathic fibrosing alveolitis	Fibroblast
172	2.18	2.87E-02	7.28E-02	GSE6955	Homo sapiens	Rett Syndrome	frontal cortex
173	2.13	3.24E-02	8.12E-02	GSE1017	Homo sapiens	Myopathy NOS	Skeletal muscle
174	2.13	3.39E-02	8.45E-02	GSE2429	Homo sapiens	Breast Cancer	Mammary Gland Tissue
175	2.12	3.57E-02	8.79E-02	GSE6764	Homo sapiens	Hepatocellular dysplasia	Liver
176	2.11	3.64E-02	8.92E-02	GSE4516	Rattus norvegicus	Smoke inhalation	Lung Tissue
177	2.1	3.41E-02	8.45E-02	GSE567	Homo sapiens	Essential Thrombocytemia	Megakaryocyte
178	2.09	3.92E-02	9.39E-02	EXPE-TABM-176	Homo sapiens	Irritable bowel syndrome variant of childhood with constipation	Sigmoid colon
179	2.08	3.69E-02	8.99E-02	GSE4130	Rattus norvegicus	Dehydration	Pituitary Gland
180	2.07	3.72E-02	9.01E-02	GSE9006	Homo sapiens	Type 2 diabetes mellitus	Peripheral blood mononuclear cell
181	2.06	4.00E-02	9.40E-02	GSE2899	Mus musculus	Type 2 diabetes mellitus	Soleus Muscle
182	2.06	4.01E-02	9.40E-02	GSE3125	Rattus norvegicus	Dehydration	Hypothalamus
183	2.06	3.99E-02	9.40E-02	GSE3407	Homo sapiens	Cockayne Syndrome	Fibroblast
184	2.06	3.79E-02	9.13E-02	GSE2866	Mus musculus	Gamma-hydroxybutyric acidaemia	Hippocampus
185	2.05	4.07E-02	9.49E-02	GSE2077	Homo sapiens	Protozoan Infection	Intestinal Epithelium

186	2.05	4.14E-02	9.60E-02	GSE9006	Homo sapiens	Type 1 diabetes mellitus	Peripheral blood mononuclear cell
187	2.03	4.01E-02	9.40E-02	GSE10123	Homo sapiens	Premature aging	Skin fibroblast
188	2.01	4.45E-02	1.01E-01	GSE3365	Homo sapiens	Crohn's disease	Peripheral blood mononuclear cell
189	2.01	4.33E-02	9.99E-02	GSE1297	Homo sapiens	Alzheimer's Disease	Hippocampus
190	2	4.40E-02	1.01E-01	GSE2254	Mus musculus	Type 1 diabetes mellitus	pancreatic islet
191	2	4.57E-02	1.03E-01	GSE3489	Homo sapiens	HIV encephalitis	frontal cortex
192	2	4.44E-02	1.01E-01	GSE3203	Mus musculus	Influenza	B Cell Lymphocyte
193	1.99	4.67E-02	1.05E-01	GSE2559	Homo sapiens	Pulmonary hypertension, primary	Pulmonary Artery
194	1.98	4.76E-02	1.06E-01	GSE3807	Homo sapiens	Aplastic anaemia	Bone Marrow
195	1.98	4.85E-02	1.07E-01	GSE4105	Rattus norvegicus	Myocardial Infarction	Myocardial tissue
196	1.96	4.72E-02	1.06E-01	GSE4479	Mus musculus	Sepsis	Splenocyte
197	1.95	5.26E-02	1.15E-01	GSE3676	Mus musculus	Infertility due to azoospermia	Testicular Tissue
198	1.94	5.21E-02	1.15E-01	GSE10064	Homo sapiens	MS (Multiple Sclerosis)	B Cell Lymphocyte
199	1.93	5.48E-02	1.17E-01	GSE5090	Homo sapiens	Polycystic Ovary Syndrome	Adipose tissue
200	1.93	5.43E-02	1.17E-01	GSE11	Mus musculus	Type 1 diabetes mellitus	Thymic epithelial cell
201	1.92	5.28E-02	1.15E-01	GSE582	Mus musculus	Transplanted Heart Complication	Myocardial tissue
202	1.92	5.44E-02	1.17E-01	GSE10586	Homo sapiens	Type 1 diabetes mellitus	T lymphocyte
203	1.92	5.77E-02	1.21E-01	GSE2049	Homo sapiens	AML - Acute myeloid leukemia	Haematopoietic stem cell
204	1.91	5.56E-02	1.18E-01	GSE11208	Homo sapiens	Nicotine addiction	Ganglioneuroblastoma
205	1.91	5.61E-02	1.18E-01	GSE5538	Mus musculus	Hepatic lipidosis	Hepatic Tissue
206	1.9	5.37E-02	1.16E-01	EXPE-MEXP-692	Homo sapiens	Barrett Esophagus	Esophagus
207	1.9	5.60E-02	1.18E-01	GSE1659	Mus musculus	Type 1 diabetes mellitus	Muscle - Striated (Skeletal) (MMHCC)
208	1.89	6.00E-02	1.25E-01	GSE4170	Homo sapiens	CML - Chronic myeloid leukemia	Haematopoietic stem cell
209	1.88	6.33E-02	1.31E-01	EXPE-MEXP-692	Homo sapiens	Adenocarcinoma of esophagus	Esophagus
210	1.86	6.21E-02	1.29E-01	GSE422	Mus musculus	Carcinoma in situ of small intestine	Intestinal Epithelium
211	1.82	6.93E-02	1.41E-01	GSE1822	Homo sapiens	Ewing's sarcoma	Renal Tissue
212	1.81	6.69E-02	1.37E-01	GSE755	Homo sapiens	Osteolysis	Leukocyte - Lymphocyte - B-Lymphocyte - Plasma Cell (MMHCC)
213	1.81	6.60E-02	1.36E-01	GSE3004	Homo sapiens	Asthma, allergic	Bronchial epithelium
214	1.78	7.26E-02	1.47E-01	GSE4060	Homo sapiens	ACTH-dependent Cushing syndrom	Adrenal gland
215	1.76	7.71E-02	1.54E-01	GSE4120	Mus musculus	Arrhythmogenic Right Ventricular Cardiomyopathy	Myocardial tissue
216	1.76	8.01E-02	1.59E-01	GSE3790	Homo sapiens	Huntington's Disease	frontal cortex
217	1.76	7.70E-02	1.54E-01	GSE9800	Homo sapiens	Cardiomyopathy, Dilated	Myocardial tissue

218	1.71	8.68E-02	1.70E-01	GSE3915	Mus musculus	Cancer of the Intestine	Small bowel
219	1.69	9.30E-02	1.80E-01	GSE5581	Mus musculus	Retinoschisis	Retina
220	1.68	8.96E-02	1.75E-01	GSE868	Mus musculus	Familial hypophosphataemic rickets	Renal Tissue
221	1.68	8.99E-02	1.75E-01	EXPE-TABM-176	Homo sapiens	IBS - Irritable bowel syndrome	Sigmoid colon
222	1.66	9.61E-02	1.85E-01	GSE6965	Homo sapiens	Infection by Aspergillus fumigatus	Dendritic cell
223	1.66	9.71E-02	1.87E-01	GSE6012	Homo sapiens	Eczema	Integument
224	1.65	9.80E-02	1.87E-01	GSE3554	Mus musculus	Glaucoma	Retina
225	1.65	1.00E-01	1.90E-01	GSE2223	Homo sapiens	Glioblastoma	CNS - Brain (MMHCC)
226	1.63	9.98E-02	1.90E-01	EXPE-TABM-26	Homo sapiens	Cancer of prostate	Prostate
227	1.62	1.03E-01	1.94E-01	GSE4172	Homo sapiens	Viral cardiomyopathy	Myocardial tissue
228	1.6	1.08E-01	2.01E-01	GSE2191	Homo sapiens	AML - Acute myeloid leukemia	Mononuclear Leukocyte
229	1.6	1.08E-01	2.01E-01	GSE2155	Homo sapiens	Breast Cancer	Epithelial Cell
230	1.56	1.18E-01	2.16E-01	GSE1299	Homo sapiens	Breast Cancer	Mammary Epithelium
231	1.55	1.15E-01	2.13E-01	GSE3320	Homo sapiens	COPD - Chronic obstructive pulmonary disease	Bronchial epithelium
232	1.55	1.19E-01	2.17E-01	GSE5774	Homo sapiens	Nonspecific interstitial pneumonia	Lung Tissue
233	1.55	1.18E-01	2.16E-01	GSE6710	Homo sapiens	Psoriasis vulgaris	Skin tissue
234	1.53	1.29E-01	2.31E-01	GSE4250	Homo sapiens	Hereditary gingival fibromatosis	Gingiva
235	1.53	1.24E-01	2.25E-01	GSE5364	Homo sapiens	Cancer of thyroid	Thyroid
236	1.53	1.18E-01	2.16E-01	GSE3583	Mus musculus	Huntington's Disease	CNS - Brain - Striatum (MMHCC)
237	1.52	1.30E-01	2.32E-01	GSE12654	Homo sapiens	Bipolar Disorder	Cerebral cortex
238	1.52	1.29E-01	2.31E-01	GSE973	Homo sapiens	Funisitis	Umbilical Blood
239	1.51	1.32E-01	2.34E-01	GSE12649	Homo sapiens	Bipolar Disorder	Cerebral cortex
240	1.5	1.33E-01	2.35E-01	GSE925	Rattus norvegicus	Cardiac Hypertrophy	cardiomyocyte
241	1.48	1.38E-01	2.42E-01	GSE3544	Mus musculus	MODY - Maturity onset diabetes in youth type 1	pancreatic islet
242	1.47	1.42E-01	2.46E-01	GSE420	Homo sapiens	Atherosclerosis	Aorta Smooth Muscle Tissue
243	1.47	1.37E-01	2.42E-01	GSE422	Mus musculus	Adenoma of small intestine	Intestinal Epithelium
244	1.46	1.41E-01	2.46E-01	EXPE-TABM-36	Homo sapiens	Hepatocellular Adenoma	Hepatocyte
245	1.45	1.38E-01	2.42E-01	GSE4302	Homo sapiens	Asthma	Epithelial Cell
246	1.45	1.44E-01	2.50E-01	GSE5370	Homo sapiens	Dermatomyositis	Muscle - Striated (Skeletal) (MMHCC)
247	1.42	1.53E-01	2.61E-01	GSE2172	Mus musculus	Colitis	Intestine - Large Intestine - Colon (MMHCC)
248	1.41	1.55E-01	2.63E-01	GSE11750	Homo sapiens	Senescence	Muscle - Striated (Skeletal) (MMHCC)

249	1.41	1.56E-01	2.63E-01	GSE3	Homo sapiens	Chromophobe Cell Carcinoma of Kidney	Renal cell
250	1.41	1.52E-01	2.61E-01	GSE2705	Homo sapiens	Primary open angle glaucoma	Optic Disk
251	1.37	1.68E-01	2.80E-01	GSE3860	Homo sapiens	Progeria	Fibroblast
252	1.37	1.73E-01	2.86E-01	GSE674	Homo sapiens	Senescence	Muscle - Striated (Skeletal) (MMHCC)
253	1.36	1.72E-01	2.84E-01	GSE2549	Homo sapiens	Malignant mesothelioma of pleura	Pleura
254	1.36	1.71E-01	2.84E-01	GSE1466	Homo sapiens	Lymphoblastic leukemia	T lymphocyte
255	1.33	1.82E-01	2.97E-01	GSE1611	Mus musculus	Down Syndrome	CNS - Brain - Cerebellum (MMHCC)
256	1.33	1.79E-01	2.93E-01	GSE997	Homo sapiens	Essential Thrombocytemia	Megakaryocyte
257	1.32	1.91E-01	3.09E-01	GSE6798	Homo sapiens	Polycystic Ovary Syndrome	Skeletal muscle
258	1.32	1.83E-01	2.98E-01	GSE3790	Homo sapiens	Huntington's Disease	CNS - Brain - Cerebellum (MMHCC)
259	1.31	1.87E-01	3.03E-01	GSE2503	Homo sapiens	Actinic keratosis	Skin tissue
260	1.29	1.94E-01	3.12E-01	GSE1010	Homo sapiens	Familial combined hyperlipidaemia	lymphoblast
261	1.27	2.00E-01	3.17E-01	GSE1028	Homo sapiens	Scott syndrome	B Cell Lymphocyte
262	1.27	1.98E-01	3.16E-01	GSE5388	Homo sapiens	Bipolar Disorder	frontal cortex
263	1.27	2.00E-01	3.17E-01	GSE2067	Homo sapiens	Hepatitis C infection	Hepatocyte
264	1.26	2.04E-01	3.22E-01	GSE3280	Homo sapiens	Acute monocytic leukaemia	Blood monocyte
265	1.26	2.07E-01	3.24E-01	GSE642	Mus musculus	Type 2 diabetes mellitus	Renal Tissue
266	1.26	2.07E-01	3.24E-01	GSE5281	Homo sapiens	Alzheimer's Disease	Superior frontal gyrus
267	1.21	2.28E-01	3.54E-01	GSE11348	Homo sapiens	Rhinovirus infection	Nose
268	1.2	2.34E-01	3.61E-01	GSE7486	Homo sapiens	Epilepsy	lymphoblast
269	1.16	2.46E-01	3.74E-01	GSE3384	Mus musculus	Nemaline Myopathy	Tibialis Muscle
270	1.16	2.45E-01	3.73E-01	GSE473	Homo sapiens	Asthma	CD4-Positive Lymphocyte
271	1.16	2.45E-01	3.73E-01	GSE474	Homo sapiens	Obesity	Muscle - Striated (Skeletal) (MMHCC)
272	1.14	2.50E-01	3.78E-01	EXPE-MEXP-669	NULL	Neuroblastoma	Adrenal Cortex
273	1.12	2.62E-01	3.95E-01	GSE3889	Mus musculus	Hypercholesteremia	Hepatic Tissue
274	1.11	2.66E-01	3.97E-01	GSE2175	Homo sapiens	Adenoma of Pituitary Gland	Pituitary Gland
275	1.1	2.71E-01	4.03E-01	GSE3925	Mus musculus	Hyperreactive airway disease	Lung Tissue
276	1.09	2.79E-01	4.13E-01	GSE10162	Mus musculus	Nephrolithiasis	Kidney
277	1.09	2.62E-01	3.95E-01	GSE2470	Rattus norvegicus	Type 2 diabetes mellitus	Pancreas
278	1.08	2.77E-01	4.10E-01	GSE362	Homo sapiens	Senescence	Muscle - Striated (Skeletal) (MMHCC)
279	1.06	2.87E-01	4.23E-01	GSE2973	Mus musculus	Infection by Yersinia enterocolitica	macrophage
280	1.04	2.98E-01	4.35E-01	GSE4785	Homo sapiens	Simian Acquired Immune Deficiency Syndrome	T lymphocyte

281	1.04	2.97E-01	4.35E-01	GSE923	Homo sapiens	Pseudomonas Infection	Lung Tissue
282	1.02	3.07E-01	4.46E-01	GSE12654	Homo sapiens	Depression	Cerebral cortex
283	1.01	3.08E-01	4.47E-01	GSE2053	Homo sapiens	RA (rheumatoid arthritis)	Synovial Membrane
284	1.01	3.14E-01	4.54E-01	GSE1037	Homo sapiens	Adenocarcinoma of lung	Lung Tissue
285	1	3.18E-01	4.58E-01	GSE4333	Mus musculus	Lymphatic edema	Skin tissue
286	0.99	3.22E-01	4.62E-01	GSE10964	Mus musculus	COPD - Chronic obstructive pulmonary disease	Lung
287	0.99	3.28E-01	4.69E-01	GSE2657	Homo sapiens	Sarcoidosis	T lymphocyte
288	0.96	3.41E-01	4.81E-01	GSE1767	Homo sapiens	Huntington's Disease	Blood
289	0.96	3.35E-01	4.77E-01	GSE7753	Homo sapiens	JRA - Juvenile rheumatoid arthritis	Peripheral blood mononuclear cell
290	0.95	3.40E-01	4.81E-01	GSE4125	Homo sapiens	Adenocarcinoma of kidney	Kidney
291	0.94	3.46E-01	4.87E-01	GSE8762	Homo sapiens	Huntington's Disease	Lymphocyte
292	0.93	3.48E-01	4.88E-01	GSE5788	Homo sapiens	Leukemia, Chronic T-Cell	T lymphocyte
293	0.92	3.56E-01	4.98E-01	GSE483	Mus musculus	Asthma, allergic	Lung Tissue
294	0.91	3.58E-01	4.99E-01	GSE2566	Rattus norvegicus	Neurogenic Muscular Atrophy	Muscle - Striated (Skeletal) (MMHCC)
295	0.91	3.60E-01	4.99E-01	GSE2600	Homo sapiens	Anaplasmosis	Leukemic Cell
296	0.91	3.68E-01	5.06E-01	GSE2127	Mus musculus	Carcinoma, Hepatocellular	Hepatic Tissue
297	0.91	3.59E-01	4.99E-01	GSE2052	Homo sapiens	MCTD - Mixed connective tissue disease	Lung Tissue
298	0.84	3.85E-01	5.26E-01	GSE2276	Mus musculus	Asthma, allergic	Lung Tissue
299	0.84	4.07E-01	5.52E-01	GSE4707	Homo sapiens	Preeclampsia	Placenta
300	0.81	4.22E-01	5.68E-01	GSE3871	Homo sapiens	Androgen insensitivity syndrome	Fibroblast
301	0.81	4.17E-01	5.63E-01	GSE1606	Mus musculus	Turner Syndrome	CNS - Brain (MMHCC)
302	0.8	4.27E-01	5.70E-01	GSE1674	Mus musculus	Hypertension	Adrenal gland
303	0.8	4.28E-01	5.70E-01	GSE3195	Mus musculus	Hypoxia	Fibroblast
304	0.79	4.28E-01	5.70E-01	GSE475	Homo sapiens	COPD - Chronic obstructive pulmonary disease	Muscle - Striated (Skeletal) - Diaphragm (MMHCC)
305	0.79	4.34E-01	5.75E-01	GSE1872	Rattus norvegicus	Breast Cancer	Mammary Gland Tissue
306	0.79	4.29E-01	5.70E-01	GSE3868	Homo sapiens	Cancer of prostate	Prostate
307	0.76	4.46E-01	5.87E-01	EXPE-MEXP-669	NULL	Neuroblastoma	Adrenal Cortex
308	0.76	4.43E-01	5.85E-01	GSE5109	Homo sapiens	Obesity	Muscle - Striated (Skeletal) (MMHCC)
309	0.73	4.64E-01	6.07E-01	GSE1413	Mus musculus	Cancer of prostate	Prostate
310	0.72	4.76E-01	6.18E-01	GSE5281	Homo sapiens	Alzheimer's Disease	Middle temporal gyrus
311	0.72	4.71E-01	6.15E-01	GSE3384	Mus musculus	Nemaline Myopathy	Extensor digitorum longus muscle
312	0.69	4.89E-01	6.32E-01	GSE2223	Homo sapiens	Astrocytoma	CNS - Brain (MMHCC)

313	0.68	4.97E-01	6.42E-01	EXPE-MEXP-476	Homo sapiens	Cancer of prostate	Endothelial cell
314	0.68	4.99E-01	6.42E-01	EXPE-MEXP-476	Homo sapiens	Cancer of prostate	Endothelial cell
315	0.66	5.10E-01	6.54E-01	GSE9877	Homo sapiens	Sickle Cell Anemia	Endothelial cell
316	0.65	5.18E-01	6.62E-01	GSE3026	Homo sapiens	Bacterial Infection	Peripheral blood mononuclear cell
317	0.63	5.30E-01	6.76E-01	GSE128	Mus musculus	Retinitis Pigmentosa	Retina
318	0.61	5.34E-01	6.77E-01	GSE1379	Homo sapiens	Breast Cancer	Mammary Gland Tissue
319	0.58	5.63E-01	7.02E-01	GSE867	Mus musculus	Hepatitis, Autoimmune	Hepatic Tissue
320	0.58	5.63E-01	7.02E-01	GSE465	Homo sapiens	Duchenne muscular dystrophy (DMD)	Muscle - Striated (Skeletal) (MMHCC)
321	0.58	5.61E-01	7.02E-01	GSE1871	Mus musculus	Acute Lung Injury	Lung Tissue
322	0.57	5.65E-01	7.02E-01	GSE5900	Homo sapiens	Monoclonal gammopathy of undetermined significance (MGUS)	Bone Marrow
323	0.57	5.70E-01	7.02E-01	GSE2223	Homo sapiens	Oligodendroglioma	CNS - Brain (MMHCC)
324	0.57	5.65E-01	7.02E-01	GSE1055	Rattus norvegicus	Cardiac Hypertrophy	cardiomyocyte
325	0.57	5.70E-01	7.02E-01	GSE4748	Homo sapiens	Bacterial Infection	Dendritic cell
326	0.57	5.73E-01	7.03E-01	GSE3384	Mus musculus	Nemaline Myopathy	Muscle - Striated (Skeletal) - Diaphragm (MMHCC)
327	0.57	5.70E-01	7.02E-01	GSE2236	Mus musculus	Congestive heart disease	Myocardial tissue
328	0.56	5.74E-01	7.03E-01	GSE1008	Mus musculus	Duchenne muscular dystrophy (DMD)	Extraocular muscle
329	0.53	5.90E-01	7.15E-01	GSE1472	Mus musculus	Duchenne muscular dystrophy (DMD)	Extraocular muscle
330	0.53	6.02E-01	7.20E-01	GSE85	Mus musculus	APECED - Autoimmune polyendocrinopathy-candidiasis-ectodermal dystrophy	Thymic epithelial cell
331	0.53	5.92E-01	7.15E-01	GSE1849	Homo sapiens	Sickle Cell Anemia	Pulmonary Artery
332	0.52	5.99E-01	7.19E-01	GSE3311	Rattus norvegicus	Alcohol poisoning	Pancreas
333	0.51	6.03E-01	7.21E-01	GSE2503	Homo sapiens	Squamous cell carcinoma	Skin tissue
334	0.5	6.17E-01	7.35E-01	GSE2899	Mus musculus	Type 2 diabetes mellitus	Hepatic Tissue
335	0.48	6.26E-01	7.42E-01	GSE1739	Homo sapiens	Severe acute respiratory syndrome (SARS)	Peripheral blood mononuclear cell
336	0.46	6.46E-01	7.57E-01	GSE5900	Homo sapiens	Smoldering multiple myeloma	Bone Marrow
337	0.45	6.64E-01	7.74E-01	GSE4678	Mus musculus	Ventricular hypertrophy	Myocardial tissue
338	0.43	6.63E-01	7.74E-01	GSE4128	Mus musculus	Adenovirus infection	Hepatic Tissue
339	0.42	6.79E-01	7.81E-01	GSE11889	Homo sapiens	CML - Chronic myeloid leukemia	Haematopoietic stem cell
340	0.42	6.72E-01	7.79E-01	GSE2779	Homo sapiens	Vitamin B 12 Deficiency	Bone marrow stem cell
341	0.4	6.89E-01	7.90E-01	GSE3	Homo sapiens	Clear cell carcinoma of kidney	Renal cell
342	0.38	7.02E-01	7.97E-01	GSE9692	Homo sapiens	Septic Shock	Whole blood

343	0.38	7.10E-01	8.01E-01	GSE6740	Homo sapiens	HIV - Human immunodeficiency virus infection	T lymphocyte
344	0.36	7.13E-01	8.03E-01	GSE121	Homo sapiens	Type 2 diabetes mellitus	Muscle tissue
345	0.36	7.25E-01	8.14E-01	GSE1402	Homo sapiens	Spondyloarthropathy	Peripheral blood mononuclear cell
346	0.34	7.34E-01	8.20E-01	GSE2271	Mus musculus	Hypoxia	Heart
347	0.34	7.40E-01	8.21E-01	GSE2466	Homo sapiens	Lymphocytic Leukemia, Chronic, B Cell	PBL (peripheral blood lymphocyte)
348	0.34	7.37E-01	8.21E-01	GSE1751	Homo sapiens	Huntington's Disease	Blood
349	0.28	7.76E-01	8.48E-01	GSE10211	Mus musculus	Sendai virus infection	Tracheal epithelium
350	0.27	7.86E-01	8.57E-01	GSE2379	Homo sapiens	Hypopharyngeal Cancer	Pharynx
351	0.25	8.01E-01	8.70E-01	GSE2884	Rattus norvegicus	Neurological pain disorder	Dorsal Root Ganglia
352	0.24	8.02E-01	8.70E-01	GSE1560	Mus musculus	Atherosclerosis	Aorta Smooth Muscle Tissue
353	0.19	8.51E-01	9.11E-01	GSE18803	Rattus norvegicus	Neurological pain disorder	CNS - Spinal Cord (MMHCC)
354	0.17	8.63E-01	9.18E-01	GSE1124	Homo sapiens	Malaria	Blood
355	0.17	8.69E-01	9.19E-01	EXPE-MEXP-1050	Homo sapiens	IUGR - Intrauterine growth retardation	Decidua basalis
356	0.15	8.82E-01	9.28E-01	GSE4697	Mus musculus	Obesity	Adipose tissue
357	0.12	9.02E-01	9.43E-01	GSE3249	Mus musculus	Leber congenital amaurosis	Retina
358	0.12	9.02E-01	9.43E-01	GSE1852	Mus musculus	Marfan Syndrome	Myocardial tissue
359	0.08	9.34E-01	9.66E-01	GSE7654	Rattus norvegicus	Hepatitis	Liver
360	0.08	9.35E-01	9.66E-01	GSE2504	Homo sapiens	HIV - Human immunodeficiency virus infection	T lymphocyte
361	0.08	9.39E-01	9.66E-01	GSE1710	Homo sapiens	Ulcerative Colitis	Sigmoid colon
362	0.08	9.40E-01	9.66E-01	GSE3167	Homo sapiens	Urothelial carcinoma	Urothelium
363	0.07	9.45E-01	9.66E-01	GSE5281	Homo sapiens	Alzheimer's Disease	Entorhinal cortex
364	0.07	9.46E-01	9.66E-01	GSE3586	Homo sapiens	Cardiomyopathy, Dilated	Myocardial tissue
365	0.04	9.70E-01	9.88E-01	GSE10758	Homo sapiens	Down Syndrome	Fetus
366	0.02	9.82E-01	9.89E-01	GSE15966	Homo sapiens	Gastrointestinal stromal tumor	Gastric Tissue
367	0.01	9.94E-01	9.96E-01	GSE11969	Homo sapiens	Small cell carcinoma of lung	Lung Tissue
368	0	9.98E-01	9.98E-01	GSE4482	Homo sapiens	Cancer of cervix	Cervix
369	-0.01	9.93E-01	9.96E-01	GSE11393	Homo sapiens	Familial combined hyperlipidaemia	Blood monocyte
370	-0.02	9.81E-01	9.89E-01	GSE10474	Homo sapiens	Acute Lung Injury	Whole blood
371	-0.02	9.81E-01	9.89E-01	GSE574	Homo sapiens	Purpura, Idiopathic Thrombocytopenic	T lymphocyte
372	-0.02	9.80E-01	9.89E-01	GSE3827	Homo sapiens	CBCL - Cutaneous B-cell lymphoma	Skin tissue
373	-0.03	9.76E-01	9.89E-01	GSE8835	Homo sapiens	B-cell chronic lymphocytic	Peripheral blood mononuclear cell

						leukaemia/small lymphocytic lymphoma	
374	-0.07	9.42E-01	9.66E-01	GSE2779	Homo sapiens	Folic Acid Deficiency	Bone marrow stem cell
375	-0.1	9.19E-01	9.54E-01	GSE860	Homo sapiens	PTSD - Post-traumatic stress disorder	Peripheral blood mononuclear cell
376	-0.11	9.18E-01	9.54E-01	GSE2935	Mus musculus	Sendai virus infection	macrophage
377	-0.11	9.15E-01	9.54E-01	GSE4483	Homo sapiens	Hypoxia	Astrocyte
378	-0.14	8.89E-01	9.34E-01	GSE1650	Homo sapiens	COPD - Chronic obstructive pulmonary disease	Lung Tissue
379	-0.16	8.74E-01	9.23E-01	EXPE-MEXP-1278	Rattus norvegicus	Arteriotomy	Carotid artery
380	-0.17	8.68E-01	9.19E-01	GSE1541	Homo sapiens	Lung Injury	Lung Tissue
381	-0.18	8.52E-01	9.11E-01	GSE2899	Mus musculus	Type 2 diabetes mellitus	pancreatic islet
382	-0.19	8.55E-01	9.12E-01	GSE935	Homo sapiens	Granulomatous Disease, Chronic	Blood neutrophil
383	-0.19	8.42E-01	9.06E-01	GSE2171	Homo sapiens	HIV - Human immunodeficiency virus infection	Peripheral blood mononuclear cell
384	-0.2	8.46E-01	9.08E-01	GSE4036	Homo sapiens	Schizophrenia	CNS - Brain - Cerebellum (MMHCC)
385	-0.22	8.27E-01	8.93E-01	GSE14245	Homo sapiens	Malignant tumor of pancreas	saliva
386	-0.24	8.06E-01	8.72E-01	GSE2459	Mus musculus	Hypertrophy, Left Ventricular	Myocardial tissue
387	-0.29	7.69E-01	8.44E-01	GSE1818	Homo sapiens	Cancer of the testis	Testis
388	-0.29	7.71E-01	8.44E-01	GSE10789	Homo sapiens	Leukemia, Adult T Cell	Blood monocyte
389	-0.3	7.66E-01	8.43E-01	GSE2368	Mus musculus	Ventilator-associated lung injury	Lung Tissue
390	-0.32	7.59E-01	8.38E-01	GSE11	Mus musculus	Type 1 diabetes mellitus	Splenic Tissue
391	-0.32	7.44E-01	8.24E-01	GSE2507	Mus musculus	Muscular Dystrophy	Myocardial tissue
392	-0.34	7.39E-01	8.21E-01	GSE11969	Homo sapiens	Adenocarcinoma of lung	Lung Tissue
393	-0.34	7.29E-01	8.17E-01	GSE3	Homo sapiens	Chromophil Carcinoma of Kidney	Renal cell
394	-0.37	7.05E-01	7.99E-01	GSE1710	Homo sapiens	Crohn's disease	Sigmoid colon
395	-0.38	6.97E-01	7.93E-01	GSE1987	Homo sapiens	Squamous cell carcinoma	Lung Tissue
396	-0.4	6.96E-01	7.93E-01	GSE1719	Homo sapiens	Macular degeneration	Fibroblast
397	-0.4	6.91E-01	7.90E-01	GSE2737	Homo sapiens	Psoriasis vulgaris	Epidermis
398	-0.41	6.78E-01	7.81E-01	GSE2729	Homo sapiens	Rotavirus infection of children	Peripheral blood mononuclear cell
399	-0.41	6.78E-01	7.81E-01	GSE14577	Homo sapiens	CFS (chronic fatigue syndrome)	Peripheral blood mononuclear cell
400	-0.43	6.66E-01	7.74E-01	GSE363	Mus musculus	Atherosclerosis	Hepatic Tissue
401	-0.46	6.46E-01	7.57E-01	GSE1987	Homo sapiens	Adenocarcinoma of lung	Lung Tissue
402	-0.47	6.42E-01	7.57E-01	GSE1786	Homo sapiens	Senescence	Muscle - Striated (Skeletal) (MMHCC)
403	-0.47	6.33E-01	7.48E-01	GSE2018	Homo sapiens	Lung transplant rejection	Lung Tissue

404	-0.49	6.26E-01	7.42E-01	GSE5113	Mus musculus	Intestinal flagellate infection	Small Intestinal Lamina Propria
405	-0.52	5.99E-01	7.19E-01	GSE4646	Homo sapiens	Meningococcal infection	Umbilical vein
406	-0.54	5.89E-01	7.15E-01	GSE3934	Homo sapiens	Meningococcal infection	Blood
407	-0.54	5.86E-01	7.13E-01	GSE11969	Homo sapiens	Squamous cell carcinoma of lung	Lung Tissue
408	-0.55	5.80E-01	7.08E-01	GSE3606	Homo sapiens	Overexertion	Leukocyte
409	-0.59	5.55E-01	6.99E-01	GSE2378	Homo sapiens	Glaucoma	Astrocyte
410	-0.61	5.43E-01	6.86E-01	GSE11969	Homo sapiens	Large cell carcinoma of lung	Lung Tissue
411	-0.63	5.34E-01	6.77E-01	GSE1907	Homo sapiens	Sarcoidosis	Blood Corpuscle
412	-0.7	4.74E-01	6.17E-01	GSE3100	Mus musculus	Cystic Fibrosis	Lung
413	-0.74	4.62E-01	6.07E-01	GSE7277	Mus musculus	Arthritis	frontal cortex
414	-0.85	3.97E-01	5.39E-01	GSE3384	Mus musculus	Nemaline Myopathy	Gastrocnemius Muscle
415	-0.85	3.95E-01	5.38E-01	GSE1363	Mus musculus	Primary pulmonary hypoplasia	Lung Tissue
416	-0.86	3.85E-01	5.26E-01	GSE11886	Homo sapiens	Ankylosing Spondylitides	macrophage
417	-0.9	3.66E-01	5.05E-01	GSE1542	Homo sapiens	Duct cell carcinoma	Pancreas
418	-0.94	3.40E-01	4.81E-01	GSE3414	Mus musculus	SCID - Severe combined immunodeficiency	Lung Tissue
419	-1.04	2.98E-01	4.35E-01	GSE2223	Homo sapiens	Anaplastic Oligoastrocytoma	CNS - Brain (MMHCC)
420	-1.11	2.66E-01	3.97E-01	GSE1615	Homo sapiens	Polycystic Ovary Syndrome	Theca Cells
421	-1.17	2.41E-01	3.70E-01	GSE1402	Homo sapiens	Chronic polyarticular juvenile rheumatoid arthritis	Peripheral blood mononuclear cell
422	-1.18	2.37E-01	3.65E-01	GSE5786	Mus musculus	Huntington's Disease	CNS - Brain - Striatum (MMHCC)
423	-1.23	2.19E-01	3.42E-01	GSE3284	Homo sapiens	Bacterial Infection	Leukocyte
424	-1.28	2.01E-01	3.18E-01	GSE3512	Rattus norvegicus	Hyperlipidemia	Hepatic Tissue
425	-1.29	1.97E-01	3.16E-01	EXPE-MEXP-357	Rattus norvegicus	Hypertension	Left Ventricle
426	-1.36	1.75E-01	2.88E-01	GSE4630	Homo sapiens	Hypoxia	macrophage
427	-1.38	1.68E-01	2.80E-01	GSE1294	Mus musculus	Down Syndrome	CNS - Brain (MMHCC)
428	-1.39	1.61E-01	2.70E-01	GSE5112	Mus musculus	Intestinal flagellate infection	Intestinal Epithelium
429	-1.42	1.53E-01	2.61E-01	GSE2006	Homo sapiens	Essential Thrombocytemia	Thrombocyte
430	-1.44	1.46E-01	2.52E-01	GSE1402	Homo sapiens	Pauciarticular juvenile arthritis	Peripheral blood mononuclear cell
431	-1.54	1.24E-01	2.25E-01	EXPE-MEXP-1283	Homo sapiens	Hodgkins lymphoma	Peripheral blood mononuclear cell
432	-1.63	1.03E-01	1.94E-01	GSE1919	Homo sapiens	RA (rheumatoid arthritis)	Synovial Membrane
433	-1.73	8.56E-02	1.69E-01	GSE2395	Homo sapiens	Cystic Fibrosis	Bronchial epithelium
434	-1.74	8.09E-02	1.60E-01	GSE6435	Mus musculus	Bacterial Infection	Leukocyte - Monocyte - Macrophage (MMHCC)

435	-1.76	7.44E-02	1.50E-01	GSE1919	Homo sapiens	Osteoarthritis	Synovial Membrane
436	-2.77	4.80E-03	1.74E-02	GSE10121	Homo sapiens	Squamous cell carcinoma of buccal mucosa	Buccal mucosa

Table 3. Lynx1-/- plasticity signature.

RP	FC	pfp	pvalue	probe_id	symbol	mm_entrez_id	hs_entrez_id	gene_name
1.2599	6.1102	0	0	ILMN_1213274	Ydjc	69101	150223	YdjC homolog (bacterial)
26.1378	1.722	0	0	ILMN_2744660	Igh-6	NA	NA	NA
87.0435	1.5896	0.0325	0	ILMN_1259747	Il33	77125	90865	interleukin 33
79.5578	1.583	0.0233	0	ILMN_1231445	Inmt	21743	11185	indolethylamine N-methyltransferase
99.1693	1.5584	0.0189	0	ILMN_1252675	D230019G01Rik	NA	NA	NA
95.5604	1.5581	0.0267	0	ILMN_2499166	Tmem65	74868	157378	transmembrane protein 65
98.106	1.5481	0.0213	0	ILMN_1251713	Car12	76459	771	carbonic anyhydrase 12
94.6178	1.5436	0.032	0	ILMN_1244887	Gria4	NA	NA	NA
96.4906	1.5339	0.0229	0	ILMN_2649671	Ipas	53417	64344	hypoxia inducible factor 3, alpha subunit
122.0152	1.5276	0.035	0	ILMN_2680188	Bai1	107831	575	brain-specific angiogenesis inhibitor 1
137.2649	1.5013	0.04	0	ILMN_2968369	Kcnip1	70357	30820	Kv channel-interacting protein 1
128.559	1.4989	0.0418	0	ILMN_2744657	Igh-6	NA	NA	NA
135.6589	1.4911	0.0425	0	ILMN_3049896	Evi2b	NA	NA	NA
295.2115	-1.4885	0.0464	3.00E-04	ILMN_2847144	Hist1h2ak	319169	221613	histone cluster 1, H2ak
271.4427	-1.5015	0.0389	2.00E-04	ILMN_2619455	Mcat	223722	27349	malonyl CoA:ACP acyltransferase (mitochondrial)
309.8626	-1.5083	0.0494	3.00E-04	ILMN_2700265	Pex11a	18631	8800	peroxisomal biogenesis factor 11 alpha
310.3477	-1.5135	0.0487	3.00E-04	ILMN_1254828	A730014O07Rik	NA	NA	NA
306.798	-1.5145	0.049	3.00E-04	ILMN_2684693	Dusp3	72349	1845	dual specificity phosphatase 3 (vaccinia virus phosphatase VH1-related)
307.0792	-1.5179	0.0488	3.00E-04	ILMN_2869715	Nell2	54003	4753	NEL-like 2
277.2855	-1.5191	0.0393	2.00E-04	ILMN_2491589	Vgll4	232334	9686	vestigial like 4 (Drosophila)
311.6705	-1.5218	0.0487	4.00E-04	ILMN_2568488	A530089A20Rik	218914	23063	wings apart-like homolog (Drosophila)
300.5669	-1.5221	0.0474	3.00E-04	ILMN_2768841	Rab22a	NA	NA	NA
312.3161	-1.5221	0.0484	4.00E-04	ILMN_3163448	Cdh8	12564	1006	cadherin 8
261.4704	-1.5237	0.0365	2.00E-04	ILMN_1214071	Ifitm1	68713	NA	interferon induced transmembrane protein 1
273.6424	-1.5279	0.0394	2.00E-04	ILMN_2757232	Aqp4	11829	361	aquaporin 4
285.8745	-1.5314	0.0422	3.00E-04	ILMN_1241551	Nell2	54003	4753	NEL-like 2
240.2307	-1.534	0.0322	2.00E-04	ILMN_2629112	Asah3l	230379	340485	alkaline ceramidase 2
295.481	-1.5354	0.046	3.00E-04	ILMN_2688728	Pcyt1a	13026	5130	phosphate cytidylyltransferase 1, choline, alpha isoform
249.2494	-1.5366	0.0328	2.00E-04	ILMN_3151149	Cpne8	66871	144402	copine VIII
273.9191	-1.5385	0.0391	2.00E-04	ILMN_2657911	Cnot4	53621	4850	CCR4-NOT transcription complex, subunit 4

309.8885	-1.5389	0.049	3.00E-04	ILMN_1257190	2900083I11Rik	58212	NA	serine/arginine repetitive matrix 3
269.2151	-1.5392	0.0385	2.00E-04	ILMN_2639849	Cbln4	228942	140689	cerebellin 4 precursor protein
290.2289	-1.5404	0.0445	3.00E-04	ILMN_1255457	Crebbp	12914	1387	CREB binding protein
256.2379	-1.5408	0.0356	2.00E-04	ILMN_3072536	Eif5	217869	1983	eukaryotic translation initiation factor 5
242.1891	-1.542	0.0315	2.00E-04	ILMN_1249000	1500015O10Rik	78896	84417	RIKEN cDNA 1500015O10 gene
306.5435	-1.5432	0.0494	3.00E-04	ILMN_1214405	Cnksr2	245684	22866	connector enhancer of kinase suppressor of Ras 2
278.6573	-1.5516	0.0393	2.00E-04	ILMN_2751988	Kitl	17311	4254	kit ligand
274.1734	-1.5518	0.0391	2.00E-04	ILMN_2673566	Eif4ebp2	13688	1979	eukaryotic translation initiation factor 4E binding protein 2
274.7663	-1.5538	0.0391	2.00E-04	ILMN_1216085	B230387C07Rik	106585	23253	ankyrin repeat domain 12
267.3929	-1.5547	0.0379	2.00E-04	ILMN_2703913	Mtf2	17765	22823	metal response element binding transcription factor 2
218.0454	-1.5569	0.03	1.00E-04	ILMN_2535881	Macrod2	72899	140733	MACRO domain containing 2
298.574	-1.5571	0.0468	3.00E-04	ILMN_1246494	LOC381445	26422	26960	neurobeachin
240.5714	-1.5576	0.0318	2.00E-04	ILMN_1225224	Ttc14	67120	151613	tetratricopeptide repeat domain 14
257.4399	-1.5601	0.0364	2.00E-04	ILMN_1259724	Man1b	17156	10905	mannosidase, alpha, class 1A, member 2
225.5851	-1.5603	0.0305	1.00E-04	ILMN_1227376	BC042720	329178	285175	unc-80 homolog (C. elegans)
233.0899	-1.5645	0.0306	1.00E-04	ILMN_2741677	Bach1	12013	571	BTB and CNC homology 1
241.988	-1.5645	0.0319	2.00E-04	ILMN_1230312	A830054O04Rik	NA	NA	NA
309.3927	-1.5684	0.0497	3.00E-04	ILMN_2793638	H2-Tw3	NA	NA	NA
275.3065	-1.5696	0.0391	2.00E-04	ILMN_2757889	Zfp91-cntf	NA	NA	NA
225.8264	-1.5706	0.0301	1.00E-04	ILMN_2654822	Chd4	107932	1108	chromodomain helicase DNA binding protein 4
247.466	-1.5728	0.0324	2.00E-04	ILMN_2731854	Creg2	263764	200407	cellular repressor of E1A-stimulated genes 2
218.4269	-1.5755	0.0297	1.00E-04	ILMN_1221598	9330133O14Rik	NA	NA	NA
259.2859	-1.578	0.0363	2.00E-04	ILMN_1227149	Meg3	17263	NA	maternally expressed 3
245.0182	-1.579	0.032	2.00E-04	ILMN_2601176	Meg3	17263	NA	maternally expressed 3
246.2646	-1.5793	0.0323	2.00E-04	ILMN_1230605	Gm336	212285	116984	ArfGAP with RhoGAP domain, ankyrin repeat and PH domain 2
225.2295	-1.5805	0.0309	1.00E-04	ILMN_2638066	Gria3	53623	2892	glutamate receptor, ionotropic, AMPA3 (alpha 3)
224.7568	-1.5808	0.0311	1.00E-04	ILMN_1253224	Dhcr24	74754	1718	24-dehydrocholesterol reductase
204.3878	-1.5825	0.0256	1.00E-04	ILMN_2544603	2610015J01Rik	67039	NA	RNA binding motif protein 25
190.3687	-1.5853	0.0233	1.00E-04	ILMN_2593230	Mllt4	17356	4301	myeloid/lymphoid or mixed-lineage leukemia (trithorax homolog, Drosophila); translocated to, 4
190.5304	-1.5853	0.0225	1.00E-04	ILMN_2519673	Vwf	22371	7450	Von Willebrand factor homolog
194.1056	-1.5868	0.0229	1.00E-04	ILMN_1215713	Egr4	13656	1961	early growth response 4

220.9951	-1.5896	0.0293	1.00E-04	ILMN_1239599	Bat2d	226562	23215	proline-rich coiled-coil 2C
218.0063	-1.5911	0.0304	1.00E-04	ILMN_2637413	Dbpht2	386753	NA	DNA binding protein with his-thr domain
185.7923	-1.5957	0.023	1.00E-04	ILMN_1247295	Hook1	77963	51361	hook homolog 1 (Drosophila)
225.437	-1.5957	0.0309	1.00E-04	ILMN_2520582	Plxna4	243743	91584	plexin A4
204.4627	-1.6008	0.0249	1.00E-04	ILMN_2674890	Tbl1x	21372	6907	transducin (beta)-like 1 X-linked
198.2794	-1.6018	0.0238	1.00E-04	ILMN_2541675	LOC382128	319675	85459	RIKEN cDNA 5830418K08 gene
202.278	-1.6049	0.0251	1.00E-04	ILMN_2690603	Spp1	20750	6696	secreted phosphoprotein 1
204.4135	-1.6064	0.0252	1.00E-04	ILMN_1224992	Gcap14	72972	54462	coiled-coil serine rich 2
236.1982	-1.609	0.0309	2.00E-04	ILMN_1235124	Thsd4	207596	79875	thrombospondin, type I, domain containing 4
193.5829	-1.616	0.0231	1.00E-04	ILMN_2737867	Mtap1b	17755	4131	microtubule-associated protein 1B
219.8212	-1.616	0.0296	1.00E-04	ILMN_1254547	Nr4a2	18227	4929	nuclear receptor subfamily 4, group A, member 2
174.6364	-1.6168	0.0212	1.00E-04	ILMN_1235652	Usp37	319651	57695	ubiquitin specific peptidase 37
190.4584	-1.6202	0.0229	1.00E-04	ILMN_1255854	Mtap9	213582	79884	microtubule-associated protein 9
183.2527	-1.6215	0.0226	1.00E-04	ILMN_3114632	Ddx6	13209	1656	DEAD (Asp-Glu-Ala-Asp) box polypeptide 6
168.6428	-1.6221	0.0204	1.00E-04	ILMN_2561533	Vps13a	271564	23230	vacuolar protein sorting 13A (yeast)
169.7224	-1.6236	0.0204	1.00E-04	ILMN_1241229	Bat2d	226562	23215	proline-rich coiled-coil 2C
161.0071	-1.6316	0.0176	0	ILMN_1231734	Nsd1	18193	64324	nuclear receptor-binding SET-domain protein 1
228.5556	-1.6327	0.0303	1.00E-04	ILMN_1259781	A430041B07Rik	328108	23116	family with sequence similarity 179, member B
164.2141	-1.6332	0.0193	1.00E-04	ILMN_1250030	Cdc42ep1	104445	11135	CDC42 effector protein (Rho GTPase binding) 1
186.6603	-1.6332	0.0229	1.00E-04	ILMN_2795040	Hist1h2ad	NA	NA	NA
189.467	-1.6364	0.0239	1.00E-04	ILMN_1216322	Hmgcs2	15360	3158	3-hydroxy-3-methylglutaryl-Coenzyme A synthase 2
189.7896	-1.6367	0.0235	1.00E-04	ILMN_2646070	Mtap1a	17754	4130	microtubule-associated protein 1 A
173.3318	-1.6391	0.0212	1.00E-04	ILMN_1229727	Gpr123	52389	84435	G protein-coupled receptor 123
182.5954	-1.642	0.0227	1.00E-04	ILMN_2715848	Slitrk4	245446	139065	SLIT and NTRK-like family, member 4
154.7165	-1.6445	0.0157	0	ILMN_2481391	Zfp326	54367	284695	zinc finger protein 326
144.623	-1.6461	0.0132	0	ILMN_1224129	Dennd3	105841	22898	DENN/MADD domain containing 3
175.2067	-1.6461	0.0208	1.00E-04	ILMN_2445958	Tssc8	63830	NA	KCNQ1 overlapping transcript 1
201.9407	-1.6496	0.0253	1.00E-04	ILMN_3059326	Sparc	20692	6678	secreted acidic cysteine rich glycoprotein
153.5956	-1.6636	0.0154	0	ILMN_3031781	Arid5b	71371	84159	AT rich interactive domain 5B (MRF1-like)
140.1691	-1.6694	0.0126	0	ILMN_2481389	Zfp326	54367	284695	zinc finger protein 326
134.6324	-1.67	0.0109	0	ILMN_1257525	Cpeb3	208922	22849	cytoplasmic polyadenylation element binding protein 3
135.784	-1.6706	0.0108	0	ILMN_1237548	5830407P18Rik	NA	NA	NA
158.0665	-1.6714	0.0161	0	ILMN_1220048	A330086O21Rik	434089	NA	predicted gene 10010

131.7096	-1.672	0.0116	0	ILMN_1254296	Chd1	12648	1105	chromodomain helicase DNA binding protein 1
134.8336	-1.6821	0.0106	0	ILMN_2654932	Pdap1	231887	11333	PDGFA associated protein 1
156.3313	-1.6827	0.016	0	ILMN_2457731	A930010C08Rik	NA	NA	NA
124.0646	-1.6846	0.0117	0	ILMN_2747381	Ddx24	27225	57062	DEAD (Asp-Glu-Ala-Asp) box polypeptide 24
138.2192	-1.6875	0.0114	0	ILMN_1248181	Zbtb7a	16969	51341	zinc finger and BTB domain containing 7a
109.4147	-1.7232	0.0089	0	ILMN_2492395	2900064A13Rik	NA	NA	NA
127.2584	-1.7307	0.0116	0	ILMN_1251488	A430041B07Rik	328108	23116	family with sequence similarity 179, member B
93.3629	-1.7373	0.0064	0	ILMN_1218471	3-Sep	24050	55964	septin 3
93.4053	-1.747	0.0062	0	ILMN_2675914	R3hdm1	226412	23518	R3H domain containing 1
124.2134	-1.7587	0.0113	0	ILMN_2680128	Zc3h13	67302	NA	zinc finger CCCH type containing 13
80.5466	-1.7652	0.0055	0	ILMN_1239042	Ankhd1	108857	54882	ankyrin repeat and KH domain containing 1
86.1003	-1.7765	0.0054	0	ILMN_3162820	Odz4	23966	26011	teneurin transmembrane protein 4
82.5619	-1.7931	0.0057	0	ILMN_1236820	9430047F21Rik	NA	NA	NA
134.4843	-1.794	0.0112	0	ILMN_2750515	Fos	14281	2353	FBJ osteosarcoma oncogene
71.9896	-1.8054	0.0055	0	ILMN_1258834	Chd1	12648	1105	chromodomain helicase DNA binding protein 1
141.8688	-1.8109	0.0128	0	ILMN_3035795	Mllt3	70122	4300	myeloid/lymphoid or mixed-lineage leukemia (trithorax homolog, Drosophila); translocated to, 3
271.3241	-1.8126	0.0392	2.00E-04	ILMN_2965669	Xlr4a	NA	NA	NA
58.7952	-1.8477	0.0031	0	ILMN_2589525	Cpeb3	208922	22849	cytoplasmic polyadenylation element binding protein 3
108.4816	-1.8546	0.0093	0	ILMN_2803674	S100a9	20202	6280	S100 calcium binding protein A9 (calgranulin B)
73.6082	-1.8653	0.0057	0	ILMN_2639442	Rock2	19878	9475	Rho-associated coiled-coil containing protein kinase 2
65.4886	-1.8737	0.0032	0	ILMN_2617920	1110017D15Rik	73721	84688	RIKEN cDNA 1110017D15 gene
48.1193	-1.9436	0.0021	0	ILMN_1217776	Mll5	69188	55904	lysine (K)-specific methyltransferase 2E
53.5131	-1.9814	0.0027	0	ILMN_2702303	Ch25h	12642	9023	cholesterol 25-hydroxylase
43.2714	-2.0064	0.0015	0	ILMN_2649773	Slc38a5	209837	92745	solute carrier family 38, member 5
37.5276	-2.0092	9.00E-04	0	ILMN_1244343	B230369L08Rik	223697	25777	Sad1 and UNC84 domain containing 2
41.0522	-2.0325	0.0017	0	ILMN_1226085	Syt1	NA	NA	NA
30.3722	-2.0661	0.0011	0	ILMN_1256701	2900016B01Rik	74901	9920	kelch repeat and BTB (POZ) domain containing 11
33.181	-2.0665	0.001	0	ILMN_2778076	2210021J22Rik	72355	150383	cysteine rich, DPF motif domain containing 1
61.2262	-2.0942	0.0029	0	ILMN_2668333	Prg4	96875	NA	proteoglycan 4 (megakaryocyte stimulating factor, articular superficial zone protein)
61.9241	-2.1057	0.0033	0	ILMN_2623983	Egr2	13654	1959	early growth response 2
18.8649	-2.4826	0.0014	0	ILMN_2652500	Lrg1	76905	116844	leucine-rich alpha-2-glycoprotein 1
13.3721	-2.4851	0	0	ILMN_2654906	Mgat3	17309	4248	mannoside acetylglucosaminyltransferase 3

25.6626	-2.6212	0.0012	0	ILMN_2710905	S100a8	20201	6279	S100 calcium binding protein A8 (calgranulin A)
6.5864	-3.7552	0	0	ILMN_2712075	Lcn2	16819	3934	lipocalin 2
4.4996	-4.7574	0	0	ILMN_1243615	Gramd4	223752	23151	GRAM domain containing 4
3.677	-5.3591	0	0	ILMN_1223734	Atf4	11911	468	activating transcription factor 4
2.1886	-7.3314	0	0	ILMN_2507182	Tomm22	223696	56993	translocase of outer mitochondrial membrane 22 homolog (yeast)
1	-13.9276	0	0	ILMN_1256369	Lynx1	23936	66004	Ly6/neurotoxin 1